Genome-wide functional analysis reveals key roles for kinesins in the mammalian and mosquito stages of the malaria parasite life cycle

Mohammad Zeeshan[1*#], Ravish Rashpa[2†], David J Ferguson[3,4†], Steven Abel[5†], Zeinab Chahine[5], Declan Brady[1], Sue Vaughan[3], Carolyn A. Moores[6], Karine G. Le Roch[5], Mathieu Brochet[2], Anthony A. Holder[7] and Rita Tewari[1*]

.

[1]University of Nottingham, School of Life Sciences, Nottingham, United Kingdom.
[2]University of Geneva, Faculty of Medicine, Geneva, Switzerland.
[3]Oxford Brookes University, Department of Biological and Medical Sciences, Oxford, United Kingdom.
[4]University of Oxford, John Radcliffe Hospital, Nuffield Department of Clinical Laboratory Science, Oxford, United Kingdom.
[5]Department of Molecular, Cell and Systems Biology, University of California Riverside, 900 University Ave., Riverside, USA.
[6]Institute of Structural and Molecular Biology, Department of Biological Sciences, Birkbeck College, London, United Kingdom.
[7]The Francis Crick Institute, Malaria Parasitology Laboratory, London, United Kingdom.
[#]Current Address: Faculty of Infectious and Tropical Diseases, London School of Hygiene and Tropical Medicine, London, United Kingdom.

*****Corresponding authors

*****rita.tewari@nottingham.ac.uk (RT), *****zeeshanmf@gmail.com (MZ)

[†]These authors contributed equally

Short title: Genome-wide analysis of *Plasmodium* kinesins

Abstract

Kinesins are microtubule-based motors important in cell division, motility, polarity, and intracellular transport in many eukaryotes. However, they are poorly studied in the divergent eukaryotic pathogens- *Plasmodium spp.,* the causative agents of malaria, which manifest atypical aspects of cell division and plasticity of morphology throughout the lifecycle in both mammalian and mosquito hosts. Here we describe a genome-wide screen of *Plasmodium* kinesins, revealing diverse subcellular locations and functions in spindle assembly, axoneme formation and cell morphology. Surprisingly, only kinesin-13 is essential for growth in the mammalian host while the other eight kinesins are required during the proliferative and invasive stages of parasite transmission through the mosquito vector. In-depth analyses of kinesin-13 and kinesin-20 revealed functions in microtubule dynamics during apical cell polarity formation, spindle assembly, and axoneme biogenesis. These findings help us to understand the importance of microtubule motors and may be exploited to discover new therapeutic interventions against malaria.

Introduction

Kinesins are microtubule (MT)-based motor proteins that use energy from the hydrolysis of ATP and function in various cellular processes including intracellular transport, mitotic spindle formation and chromosome segregation during cell division, and the organisation of cell polarity and cytoskeletal features associated with motility (1, 2). In eukaryotes, there are 14 to 16 kinesin subfamilies categorised according to the primary sequences of the motor domain, with similar biological roles also established by *in vitro* studies, and *in vivo* phenotypes for subfamily members (2-4). Kinesin subfamilies that regulate MT dynamics, such as kinesin-8 and -13, are found in most eukaryotes including primitive and evolutionarily divergent eukaryotes (5, 6). Although there is an extensive kinesin literature with various bioinformatic and molecular investigations, information is sparse on these molecular motors in deep rooted pathogenic eukaryotes including *Plasmodium spp.* and other Apicomplexa, *Giardia spp.,* and trypanosomes (6). These primitive eukaryotes have a flagellate stage in their life cycle and may have a complex MT-associated cytoskeleton (7), indicating the importance of MT-based motor proteins in their development.

Plasmodium spp., the causative agents of malaria belong to the phylum Apicomplexa. They are ancient haploid unicellular eukaryotes with several morphologically diverse proliferative stages during the complex life cycle in various cells, tissues, and organs of their vertebrate and invertebrate hosts **(Fig 1A)** (8, 9). In the mammalian host the parasite proliferates within liver and red blood cells (RBC) by repeated cycles of closed mitotic division retaining an intact nuclear membrane, with cytokinesis following the final nuclear division, in a process termed schizogony, to produce multiple infective haploid merozoites **(Fig 1A)**. Some of these haploid parasites in the RBC arrest and commit to sexual development as gametocytes **(Fig 1A)**. Gametocytes develop no further into gametes unless ingested in a blood meal by a female mosquito (the invertebrate host). Male gametogenesis is very rapid and complete within 12 to 15 min after activation (10). Within the nucleus, three rounds of DNA replication and chromosome segregation produce an 8N genome, which is followed by nuclear division and cytokinesis. At the same time, in the cytoplasm axoneme assembly and maturation occur, leading to the formation of flagellate haploid male gametes in a process termed exflagellation (8, 9). The motile male gamete finds and fertilises the female gamete, and the resultant zygote differentiates through six distinct stages (I to VI) into a banana-shaped, invasive motile ookinete with a distinct apical polarity and conoid-associated proteins (8, 11, 12). At the same time, in the first stage of meiosis, the DNA is duplicated and the now tetraploid ookinete develops over a 24 h period in the mosquito gut (8, 12), before traversing the mosquito gut wall and forming an oocyst under the basal lamina. Within the oocyst, sporogony, which is a form of endomitosis, produces many haploid sporozoites (13, 14). Sporozoites are motile and invasive polarised cells that migrate to and invade the salivary glands, so that the bite of the infected mosquito injects them into the next mammalian host (15). Overall, the complete life cycle of the malaria parasite is characterised by varied morphological differences in size and shape, together with various modes of cell division and proliferation **(Fig 1A)**.

In a recent bioinformatic analysis of kinesins in Apicomplexa, we found nine kinesins encoded in the *Plasmodium berghei* genome, with members of three conserved kinesin subfamilies (kinesin-5, -8B, -8X and -13); kinesin-4, -15 and -20; and two Apicomplexa-enriched kinesins: kinesin-X3 and -X4 (16). Surprisingly, kinesin-5, -8X and -8B were not essential for blood stage proliferation (16-18). However, deletion of *kinesin-5*, which codes for a protein clearly co-located with the spindle apparatus in all

proliferative stages, affected the production of infective sporozoites (17). Kinesin-8X was required for endomitotic proliferation in oocysts, and *kinesin*-8B deletion resulted in a defect in axoneme biogenesis during male gametogenesis (16, 18, 19).

Here, we present a comprehensive genome-wide screen of all *P. berghei* kinesins, including additional analyses of previously studied kinesin-5, -8B and -8X (16-18), using gene-targeting approaches, live-cell imaging, ultrastructure expansion microscopy and electron microscopy, and RNA-seq and ChIP-seq analyses. We examine the subcellular location of each kinesin using a protein endogenously tagged at the C-terminus with GFP, revealing a differential localisation of kinesins in mitotic and meiotic stages and a pellicular and polar location in certain invasive stages. Eight of the nine kinesin genes are required only for parasite transmission through the mosquito vector, during the sexual and sporogony stages. Only kinesin-13 is likely essential during blood stage schizogony. An in-depth analysis of kinesin-13 and -20 during gametocyte and ookinete stages revealed distinct subcellular locations and functions in MT spindle assembly and formation, axoneme assembly and cell polarity. Kinesin-20 was associated with a striking ring-like structure during zygote to ookinete differentiation and deletion of the kinesin-20 gene revealed a function in the morphology and motility of the ookinete. Kinesin-13 is expressed at all proliferative stages of the life cycle, and it associates with the kinetochore. A kinesin-13 genetic knockdown affected MT dynamics during spindle formation and axoneme assembly in male gametocytes, and subpellicular MT organization in ookinetes. These findings help us understand the importance of MT motors and may be exploited to discover new therapeutic interventions against malaria.

Results

Live-cell imaging of *Plasmodium* kinesins reveals diverse locations during cell division, differentiation, and pellicle formation throughout the life cycle.

To investigate the expression and subcellular location of kinesins throughout the *P. berghei* life cycle, we generated transgenic parasite lines by single crossover recombination at the 3' end of each gene to express a fusion protein with a C-terminal GFP-tag **(S1A Fig).** PCR analysis of genomic DNA from each line, using locus-specific diagnostic primers, indicated correct integration of the GFP sequence **(S1B Fig).** Immunoprecipitation assays using GFP-trap beads and mass spectrometry analysis of at least six kinesin-GFP proteins confirmed the presence of peptides of intact fusion protein in gametocyte lysates **(S2A and B Figs).** Each kinesin-GFP parasite line completed the full life cycle with no detectable phenotypic change resulting from the GFP tagging. We analysed the expression and subcellular location of these GFP-tagged proteins by live cell imaging at various stages of the life cycle. Taken together with the previously published results for kinesin-5, -8B and -8X (16-18), we found that the nine kinesins have a diverse pattern of expression, with distinct subcellular locations including the mitotic spindle, axonemes, the surface pellicle, and a polar distribution at various stages of the parasite life cycle **(Figs 1B and 1C, and S3 Fig).** Interestingly, only two kinesins, kinesin-5 and -13, were expressed throughout the parasite life cycle, including blood stage schizogony, and were located on the mitotic spindle in both asexual and sexual stages **(S3 Fig).** Kinesin-5GFP was restricted to the nucleus, while kinesin-13GFP had both a nuclear and cytoplasmic location **(S3 Fig).** Kinesin-8XGFP was also located on the nuclear spindle but only during the proliferative stages within the mosquito vector. Three kinesins (kinesin-8B, -15 and -X4) were expressed only during male gametogenesis with cytosolic locations **(S3 Fig)**, and two kinesins (kinesin-20 and -X3) were first detected in female gametocytes with a diffuse location **(S3 Fig)**. Their presence continues into the zygote and later stages of ookinete differentiation and sporogony with locations that are discussed in detail below. We also observed two kinesins at polar locations: kinesin-8X at the basal end of stage V to VI ookinetes and kinesin-13 at the apical end throughout ookinete development **(S3 Fig).** Overall, kinesin-5 and -8X are restricted to nuclear spindle and kinesin-13 is present in both nucleus and cytoplasm **(Fig 1B and 1C)**. The Apicomplexa-enriched kinesin-X3 and -X4 are confined to ookinete and sporozoite pellicle and flagellar axoneme, respectively.

Genome-wide functional screen reveals that eight out of nine kinesins are required only for parasite transmission and not for blood stage proliferation.

Previously we described the functional roles during mosquito stages of three kinesins, -5, -8B and -8X; proteins that were not essential during blood stage development (16-18). To study the function of the remaining six kinesins throughout the life cycle, we attempted deletion of each gene from *P. berghei* using a double crossover homologous recombination strategy as described previously (20) **(S4A Fig)**. Successful integration of the targeting constructs at each gene locus was confirmed by diagnostic PCR **(S4B Fig)**, except that *kinesin-13* could not be deleted. PCR analysis of knockout parasites confirmed the complete deletion of these *kinesin* genes **(S4B Fig)**, indicating that they are not essential during the asexual blood stage. *kinesin-13*, which could not be deleted despite several attempts, likely has an essential role during the asexual blood stage **(Fig 1D).** A recent functional profiling of the *P. berghei* genome (21) also supports an essential role for kinesin-13 during the blood stage. This previous study found that five

kinesins (kinesin-4, -8B, -8X, -20 and -X4) are not essential for blood stage growth but provided no data for kinesin-5, -15 and -X3 (21).

Phenotypic analyses of the *kinesin*-knockout parasites, in comparison with the parental parasite (WTGFP), were carried out at various stages of the life cycle: in asexual blood stages, during male gametogenesis and the formation of exflagellation centres, during ookinete formation, in the number and size of oocysts, for the formation of sporozoites in oocysts and their migration to salivary glands, and for parasite transmission to the vertebrate host **(Fig 1D)**. Taken together with previously published studies on kinesin-5, -8B and -8X, only two knockout parasite lines (*Δkinesin-8B* and *Δkinesin-15*) showed a defect in the formation of male gametes **(Fig 1D, S5A Fig)**. *Δkinesin-8B* parasites produced no male gametes, as shown previously (18, 19), while there was a significant decrease in male gamete formation in *Δkinesin-15* parasites **(Fig 1D, S5A Fig).** Next, we analysed the zygote to ookinete transition (round to banana-shaped cells) after 24 h following gametocyte activation. Three parasite lines (*Δkinesin-8B, Δkinesin-15* and *Δkinesin-20*) produced no or reduced numbers of ookinetes **(S5B Fig)**. *Δkinesin-8B* parasites produced no ookinetes, as expected because there were no male gametes to fertilise the female gametes **(Fig 1D, S5B Fig**) (18). *Δkinesin-15* parasites produced significantly fewer male gametes, which would be expected to result in fewer ookinetes compared to WTGFP parasites **(Fig 1D, S5B Fig)**. In contrast, *Δkinesin-20* parasites exflagellated normally and therefore loss of this kinesin must have a direct effect on ookinete formation **(S5B Fig)**.

To assess the effect of kinesin gene deletions on oocyst development and infective sporozoite formation, 40-50 *Anopheles stephensi* mosquitoes were fed on mice infected with individual *kinesin*-knockout lines, and parasite development was examined. First, GFP-positive oocysts on the mosquito gut wall were counted at 7-, 14- and 21-days post-infection (dpi). Three out of eight kinesin-knockout lines showed defects in oocyst production; *Δkinesin-8B* parasites produced no oocysts as shown previously (18), while there was a significant reduction in *Δkinesin-15* and *Δkinesin-20* oocysts compared to WTGFP oocysts at 7 dpi and a further reduction by 14 and 21 dpi **(S5C Fig)**. The adverse effects on ookinete production rather than a direct effect on oocyst development could explain this observation. Although there was no significant difference in the number of oocysts of other kinesin gene knockouts compared to WTGFP at 7 dpi, a significant reduction was observed for the *Δkinesin-8X* line at 14 dpi, which became more evident by 21 dpi **(S5C Fig)**. Oocyst size was not affected in most of the lines that produced them, the only exception was *Δkinesin-8X* oocysts, which were approximately half the size of WTGFP oocysts at 14 dpi, and even smaller by 21 dpi **(S5D Fig)**. . Four out of eight kinesin-knockout lines produced no or defective sporozoites; *Δkinesin-8B* and *Δkinesin-8X* produced no sporozoites, as reported earlier (16, 18), while *Δkinesin-15* and *Δkinesin-20* lines had significantly reduced sporozoite numbers compared to control parental parasites **(Fig 1D, S5E Fig)**. These defects were mirrored in the salivary glands: for the *Δkinesin-8B* and *Δkinesin-8X* lines no sporozoites were detected, as reported earlier (16, 18), while *Δkinesin-15* and *Δkinesin-20* lines had a significantly reduced number. The *Δkinesin-5* parasite produced significantly fewer infective salivary gland sporozoites **(S5F Fig)** as reported previously (17). However, although several kinesin gene-knockout lines exhibited defects in sporozoite production and reduced salivary gland infection, these sporozoites were still infectious to the mammalian host as observed with successful infection of new hosts in mosquito bite back experiments **(Fig 1D, S5G Fig)**. In summary, for most of the kinesin gene-knockout *P. berghei* lines, there were clear developmental defects at specific stages of the life cycle within the mosquito vector.

Apicomplexa-enriched kinesins have discrete locations during pellicle formation (-X3) and axoneme assembly (-X4) during sexual development.

Previous bioinformatic analysis identified two divergent *Plasmodium* kinesins (kinesin-X3 and –X4) (5, 16); one of them (kinesin-X3) is restricted to the phylum Apicomplexa (16). Kinesin-X4 is also restricted to Apicomplexa except that it is also present in the starlet sea anemone *Nematostella vectensis* (5). The parasitic Apicomplexa are characterised by a specialised apical structural complex that coordinates the interaction with and penetration of host cells, and have a surface pellicle comprised of the plasma membrane and an underlying layer of fused flattened membrane vesicles of the inner membrane complex (IMC) with associated MTs (22, 23). To examine whether the kinesins are associated with these apicomplexan features, localisation by live cell imaging was performed. Kinesin-X3 and –X4 showed stage-specific expression during sexual development with a distinct location **(S3 Fig)**. During zygote to ookinete differentiation, kinesin-X3 expression was restricted to one side of the cell in the early stages of development (stage I-III), suggesting an involvement in pellicle formation **(Fig 2A)**. In later stages (stage IV-VI), the kinesin-X3 location became more distinct around the periphery of the ookinete. Monoclonal antibody 13.1 conjugated with cy3 (red), which recognises the P28 protein on the surface of zygote and ookinete stages, stained these stages and colocalised with kinesin-X3 (green) **(Fig 2A)**, although kinesin-X3 was not present at the apical and basal ends of the developing ookinete **(Fig 2A)**. The data suggest that kinesin-X3 is restricted to pellicle formation during ookinete and sporozoite stages in the mosquito.

Using real time live-cell imaging of male gametogenesis, the expression and location of kinesin-X4 (green) was compared with that of axonemal protein kinesin-8B (red) located on basal bodies and axonemes (18). Kinesin-X4 showed a diffuse cytosolic distribution during early stages of male gametogenesis (1-3 minutes post activation [mpa]) but no strong signal on the basal body tetrads labelled with kinesin-8B (red) **(Fig 2B)**. However, at 4-6 mpa the kinesin-X4 signal distribution changed to resemble linear structures, which were maintained in the later stages (8-10 mpa) and showed co-localization with kinesin-8B **(Fig 2B)**. These data suggest that kinesin-X4 is located on axonemes together with kinesin-8B during flagella formation in *Plasmodium spp.*

Kinesin-8X and -5 are nuclear spindle kinesins associated with the kinetochore (NDC80) that bind centromeres.

In our previous studies we showed that two kinesins, -5 and -8X, are associated with spindles and restricted to the nucleus during most of the life cycle stages (16, 17). Both, kinesin-8X and -5 form an arc like spindles in male gametocytes activated for 1-1.5 min and co-localises with α-tubulin **(Fig 2C)** (16, 17).To further examine the spatio-temporal dynamics of these kinesins during spindle formation, chromosome segregation and axoneme biogenesis during male gametogenesis, we crossed parasite lines expressing kinesin-8XGFP and -5GFP with lines expressing NDC80-Cherry, a kinetochore protein in the nucleus, and kinesin-8B-Cherry, an axonemal protein in the cytoplasm, and compared protein location by live-cell imaging **(S6A Fig)**. Both kinesin-8X and -5 (green) were co-localised with NDC80 (red) suggesting a role in mitotic spindle function and chromosome segregation **(Fig 2D and S6B Fig).** On the other hand, neither kinesin-5 nor kinesin-8X showed any overlap with cytosolic kinesin-8B (red) during male gametogenesis **(S6C Fig and S6D Fig)** confirming their restricted location within the nuclear compartment.

Kinetochores are multiprotein complexes assembled at the centromere of each chromosome, which mediate chromosome attachment to spindle MTs. Because kinesin-8X and -5 showed colocalization with kinetochore protein NDC80, we analysed further the binding of these proteins at the centromere DNA. We performed ChIP-seq experiments with parasites undergoing gametogenesis (6 min post-activation [mpa]), using kinesin-8XGFP and -5GFP tagged parasites and GFP-specific antibodies. Strong ChIP-seq peaks for each chromosome were observed with these kinesins, indicating their binding sites. Binding was restricted to a region close to the previously annotated centromeres of all 14 chromosomes (24) and identical to those identified in *Plasmodium* Condensin and NDC80 studies (8, 25) **(Fig 2E and S7 Fig).** Together, live cell imaging and ChIP-seq analysis support the notion that kinesin-8X and -5 associate with kinetochores assembled at centromeres.

Kinesin-20-GFP location reveals a ring-like structure during ookinete differentiation, and deletion of the kinesin-20 gene affects ookinete morphology and motility.

In the initial phenotypic screen described above, the *Δkinesin-20* parasite did not produce normal ookinetes **(S5B Fig)** but did produce a few oocysts **(S5C Fig)**, so we undertook a more in-depth analysis to investigate this further. First, we analysed the spatiotemporal profile of kinesin-20GFP expression during zygote to ookinete differentiation, using P28 as a cell surface marker. Live cell imaging showed a diffuse distribution of kinesin-20GFP in the female gametocyte and zygote **(Fig 3A, S2 Fig)**. Subsequently, the intensity of kinesin-20GFP increased in the developing apical protuberance from the main cell body, and in later stages, especially at stage-II and III that are about 6-8 h after gametocyte activation **(Fig 3A)**. The protein appeared as a ring restricted to the junction of the main cell body and the protrusion that is characteristic of developing ookinetes during stage II to stage V, and then dispersed in mature ookinetes (stage VI), with a largely diffuse distribution like that in the zygote stage **(Fig 3A)**.

Next, we examined the *Δkinesin-20* parasites to ascertain whether the zygote was formed and at what stage parasite development was blocked. The *Δkinesin-20* parasite developed a short protuberance in stage-II like that of the WTGFP control **(Fig 3B)**, but this protrusion developed into a bulbous structure rather than the characteristic banana-shaped ookinete **(Fig 3B)** and remained like this 24 h later when the banana shaped WTGFP ookinete had fully differentiated **(Fig 3B and C)**. Since the mature wildtype ookinete is a motile and invasive stage, we investigated the motility of the *Δkinesin-20* bulbous ookinete using a Matrigel substrate, as described previously (16, 26). There was a significant decrease in the motility of *Δkinesin-20* ookinetes compared with the WTGFP ookinetes that showed normal gliding motility **(Fig 3D and E; S1 movie and S2 movie)**.

Although *Δkinesin-20* parasites made no morphologically normal and motile ookinetes, nevertheless they formed a few oocysts that produced sporozoites **(S5 Fig)**. This would point to the mutation specifically affecting motility but not invasion of the mosquito gut. It is possible that a few immotile ookinetes may contact the mosquito gut wall during gut turbulence and these are able to invade and initiate oocyst formation. The *Δkinesin-20* sporozoites were morphologically like WTGFP parasites, so we examined their motility on Matrigel as described previously (26, 27). The motility of *Δkinesin-20* sporozoites was like that of WTGFP sporozoites **(S8A Fig and S8B Fig; S3 movie and S4 movie)**, suggesting that the defect in *Δkinesin-20* parasite shape and motility is limited to ookinete development.

To examine whether the expression of other kinesin genes is mis-regulated in *Δkinesin-20* gametocytes at 2h post activation, we performed qRTPCR analysis of them. We wished to check expression of other kinesins located in the cytoplasmic compartment of ookinete stages e.g. kinesin-X3 and kinesin-13 expecting that expression of other kinesins coordinated with kinesin-20 would be modulated. However, there was no significant change in expression of any other kinesin gene in *Δkinesin-20* parasites compared with WTGFP parasites **(S8C Fig)**.

To determine genome-wide changes in transcription we performed RNA-seq analysis of the *Δkinesin-20* gametocytes at 2h post activation, because kinesin-20 expression starts in female gametocytes and continues into later stages. *Plasmodium* displays translational repression in female gametocytes with de-repression only after fertilisation and translation of many proteins in the zygote (28). We wished to identify any role of kinesin-20 in translational de-repression. The *kinesin-20* deletion in the *Δkinesin-20* strain was confirmed, since no significant reads mapped to this gene locus **(S8D Fig).** We found no significant change in transcriptome due to *kinesin-20* deletion except one gene was upregulated, and 16 genes were down regulated **(S8E Fig, S1A Table)**. Most of the differentially expressed genes belong to *pir* and *fam* gene clusters located in telomeric and sub-telomeric regions of chromosomes. Two of the genes (PBANKA_1465700 and PBANKA_0200600) most downregulated in *Δkinesin-20* gametocytes belong to the *fam* gene cluster and were described as female gametocyte specific genes in a recent study (29). This suggesting a link between kinesin-20 function and female gametocyte development but no role of kinesin-20 in translational de-repression.

Ultrastructure analysis of *Δkinesin-20* ookinetes reveals disorganised subpellicular microtubules.

The unusual size and shape of *Δkinesin-20* ookinete led us to perform high resolution and ultrastructure analysis of the bulbous ookinetes using ultrastructure expansion- and electron microscopy. By expansion microscopy using tubulin-specific antibody, we observed a marked reduction in microtubule length **(Fig 3F)**: the length of MTs in *Δkinesin-20* bulbous ookinetes was decreased by approximately 40% compared to those of WTGFP parasites, reflecting a reduction in the overall length of the ookinete **(Fig 3G).** This difference was confirmed by electron microscopy observations **(Fig 4)**.

In an ultrastructural comparison of WTGFP and *Δkinesin-20* ookinetes, the most obvious difference was the shape of the cell. In longitudinal section, the WTGFP ookinetes were elongated with a crescentic outline **(Fig 4Aa)**, and, in contrast, *Δkinesin-20* ookinetes were less elongated and had a more bulbous appearance **(Fig 4Ab, c).** In WTGFP parasites, the distribution of subcellular organelles was ordered with most micronemes in the apical cytoplasm, a more centrally located crystalline body and a posterior nucleus **(Fig 4Aa).** In contrast, early *Δkinesin-20* ookinetes had a large central nucleus with a few dense granules but lacked both micronemes and a crystalline body **(Fig 4Ab).** Others that appeared more mature, possessed similar organelles (micronemes, crystalline body, nucleus) to those of the WTGFP, but differed from the control in having more randomly distributed micronemes **(Fig 4Ac)**.

Due to the differences in cell shape, the apical complex and pellicle were examined in detail. When the apical complex was examined in longitudinal **(Fig 4Ad, e)** and cross **(Fig 4Af, g)** section, the complex nature of the structure was revealed. Interestingly, WTGFP and *Δkinesin-20* ookinetes displayed an identical sub-structure **(Fig 4Ad–e and f–g).** In longitudinal sections of the central apex region, three conoidal rings could be identified underneath the plasma membrane. A unique sub-structure of

the ookinete is the apical collar, which represents a cone-like structure embedded between the microtubules and IMC of the pellicle (11). The outer region of the collar is electron dense and appears to be fused to the IMC, which is interrupted at the apical end to form apical polar ring 1 **(Fig 4Ad-g).** The inner aspect of the collar is more electron lucent and in close contact with the sub-pellicular MTs **(Fig 4Ad-g)**. The apical ends of the MTs are attached to a ring forming apical polar ring 2 **(Fig 4Ad, e).** For a detailed review of the apical complex see Koreny et al (11). Approximately 50 sub-pellicular MTs emanate from polar ring 2 and run longitudinally beneath the collar **(Fig 4Af, g)** and then beneath the IMC of the pellicle **(Fig 4Ah, i).** In the region of the collar, MTs were evenly distributed in both WTGFP and *Δkinesin-20* parasites **(Fig 4Af, g).** However, in more posterior sections, while there continued to be an even distribution of MTs in close contact with the IMC in the WTGFP ookinete **(Fig 4Ah)**, in the *Δkinesin-20* parasite there were areas where there was uneven distribution, clumping and detachment of MTs from the IMC **(Fig 4Ai).** A schematic of the ookinete apical end is given in **Fig 4B**. It shows that sub-structures of the apical complex (i) are identical in both WTGFP and *Δkinesin-20* parasite. The microtubules in the region of the collar (ii) are evenly distributed, but they are unevenly distributed, clumped and detached in posterior sections (iii) of *Δkinesin-20* ookinetes.

Kinesin-13 associates with kinetochore marker NDC80 at all proliferative stages of the life cycle and its knockdown affects male gamete formation.

Since the kinesin-13 gene was the only kinesin gene essential for blood stage schizogony and could not be disrupted in our genome-wide screen **(Fig 1D and S5 Fig)**, we made a detailed analysis of the protein. We observed both a diffuse cytoplasmic distribution and a distinct nuclear pattern of kinesin-13GFP in all proliferative stages as shown in **Fig 1C and S2 Fig**. We performed live cell co-imaging of kinesin-13GFP and the NDC80-cherry kinetochore marker after crossing the two transgenic parasite lines, to observe kinesin13-GFP dynamics during chromosome segregation in various developmental stages. There was colocalization of kinesin-13 and NDC80 at all proliferative stages **(Fig 5)**, for example during the schizogony and sporogony endomitotic stages **(Fig 5A, B)**. In the sexual cells, during the rapid mitosis of male gametogenesis there was partial colocalization of kinesin-13 and NDC80, but a substantial amount of kinesin-13 was also located in the cytosolic compartment **(Fig 5C).** In the meiotic stage during ookinete development there was clear colocalization of kinesin-13 and NDC80 **(Fig 5D)**. At the start of meiosis (2 h after zygote formation) there was one strong nuclear focus and at the end of ookinete formation there were three to four co-localised foci (**Fig 5D).** To further examine the location of kinesin-13, we used ultrastructure expansion microscopy to examine gametocytes activated for 15 min, and then compared its location with that of tubulins. Kinesin-13 (green) was observed to co-localize with α/β tubulin (magenta) suggesting a location on axonemes and spindles **(Fig 6A)**. Further analysis of the male gamete by fixed immunofluorescence microscopy revealed a colocalization of kinesin-13 (green) with tubulin (red) **(Fig 6B).**

Since kinesin-13 is essential for the asexual blood stage, and the gene could not be deleted, we applied two conditional genetic knockdown strategies to evaluate its role at other proliferative stages within the mosquito vector. First, we used an auxin-inducible degron (AID) system to try and study the effect of rapid kinesin-13 degradation in gametocytes. We tagged the endogenous kinesin-13 gene with an AID/HA epitope tag **(S9A Fig)** to degrade the fusion protein in presence of auxin (30), and successfully generated kinesin-13-AID parasite lines as shown by integration PCR **(S9B Fig)** but could not deplete kinesin-13 protein by auxin treatment **(S9C Fig)**. Next, we used a

promotor trap double homologous recombination (PTD) approach, inserting the *clag* promotor at the 5' end of kinesin-13, and generated the conditional knockdown parasite: P*clag*kinesin-13 (kinesin-13PTD) **(S9D Fig)**. *clag* (cytoadherence-linked asexual gene) is highly expressed in asexual blood stages, but largely silent during stages of sexual differentiation, including gametocytes and ookinetes (31). The successful insertion was confirmed by diagnostic PCR **(S9E Fig)** and qRT PCR showed a significant downregulation of kinesin-13 gene transcripts in *kinesin-13PTD* gametocytes, when compared to WTGFP gametocytes **(Fig 6C).**

The phenotype of the *kinesin-13PTD* modification was examined during various stages of the parasite life cycle. Parasite proliferation in asexual blood stages was not affected, but during male gametogenesis, exflagellation was markedly reduced and very few male gametes were produced by *kinesin-13PTD* parasites compared to WTGFP parasites **(Fig 6D).** Zygote development and ookinete differentiation were severely affected, and no clear banana-shaped ookinetes were observed **(Fig 6E).** Subsequent stages in the mosquito were also affected significantly and no oocyst or sporozoite formation was observed **(S7F Fig)**, and consequently no transmission of *kinesin-13PTD* parasites occurred, as shown by mosquito bite back experiments **(S9G Fig).**

Global transcriptomic analysis of *kinesin-13PTD* parasites shows mis-regulation of transcripts for gene clusters involved in axoneme assembly and chromosome dynamics.

To examine the transcript level of other kinesins in *kinesin-13PTD* gametocytes, we performed qPCR for all the nine kinesins and found that some, like kinesin-8B, -8X, -15 and -20, were downregulated **(Fig 6F).**

Since transcripts of other kinesins were affected, global transcription was investigated by RNA-seq analysis of *kinesin-13PTD* gametocytes at 0 and 15 mpa, representing times point before the start of male gametogenesis and just after male gamete formation (exflagellation), respectively. *Kinesin-13* downregulation in *kinesin-13PTD* gametocytes, relative to WTGFP gametocytes, was confirmed by RNA-seq analysis, showing the lack of reads for this locus **(Fig 6G).** In addition to reduced kinesin-13 expression, 34 other genes were significantly downregulated and the expression of 152 genes was significantly upregulated in *kinesin-13PTD* gametocytes before activation (at 0 mpa) **(Fig 6H; S1B Table).** Similarly, the expression of 22 genes was significantly downregulated and the expression of 329 genes was significantly upregulated in *kinesin-13PTD* gametocytes after 15 min activation **(Fig 6I; S1C Table).** Bioinformatic analysis of these differentially regulated genes revealed two important clusters of genes that were affected, including those coding for proteins involved in axoneme assembly, glideosome assembly and chromosome dynamics **(Fig 6J).**

High resolution ultrastructure analysis of *kinesin-13PTD* parasites identifies defects in spindle assembly and axoneme MT of gametocytes, and the subpellicular MT of ookinetes.

Phenotypic analysis of *kinesin-13PTD* parasites revealed defects in male gamete and ookinete formation, and therefore we performed comparative high-resolution image analysis of *kinesin-13PTD* and WTGFP gametocytes and ookinetes. Ultrastructure expansion microscopy revealed that both spindle and axoneme MTs were disorganized, and no clear flagella were visible at 4 to 5 or 15 min after male gametocyte activation, respectively **(Fig 7A).** Disorganized MT were also observed in the defective *kinesin-13PTD* zygotes/ookinetes in comparison to the corresponding WTGFP parasites **(Fig 7A).**

These data were substantiated by electron microscopy analysis of male gametocytes activated for 6 or 15 min **(Fig 7B)**. The electron micrographs showed that in both WTGFP and *kinesin-13PTD* parasites at 6 mpa, most male gametocytes were at an early stage of development, with a spherical appearance and a large central nucleus **(Fig 7Ba, c).** In WTGFP gametocytes, several nuclear poles (also known as spindle poles) were observed while the cytoplasm contained several normal 9+2 axonemes, and some abnormal axonemes **(Fig 7Ba, b).** Although in the *kinesin-13PTD* gametocytes few nuclear poles were observed **(Fig 7Bc)**, the major difference was in the cytoplasm, where there were collections of free single and double MTs plus several partially organized into axoneme-like structures **(Fig 7Bd)** while 9+2 axonemes were very rare. At 15 mpa, in the WTGFP samples, several late stages were observed with evidence of exflagellation and protruding microgametes **(Fig 7Be)** and several free male gametes complete with nucleus and flagellum were observed **(Fig 7Bf, g).** In contrast, in the *kinesin-13PTD* parasites, most male gametocytes were still at an early stage, and in the few at a later stage, the nucleus displayed clumps of chromatin **(Fig 7Bh)** with a few examples of protrusions of MTs from the plasma membrane **(Fig 7Bi),** but with no evidence of flagella formation or free male gametes.

Discussion

Plasmodium spp. have a complex life cycle involving two hosts. They invade tissues and cells in diverse environments and have evolved a series of cellular shapes and sizes, with several distinct morphological forms with cellular polarity and gliding motility for invasion, and cellular proliferation underpinned with an atypical mode of cell division (8, 9, 32). Many of these processes are governed by MTs and MT-based motor proteins like kinesins (16). In many organisms including *Plasmodium spp.,* MTs form different structural frameworks such as the spindle assembly during cell division, the axonemes of cilia and flagella, and a cytoskeletal scaffold to establish and maintain cell polarity, cell shape, intracellular transport, and cell motility (33, 34). Kinesins regulate the organisation and function of MTs, using them as a track for movement or regulating their dynamics during cellular processes (1, 6). *Plasmodium spp*. are evolutionarily divergent unicellular eukaryotes with genomes that encode nine kinesins including two that are Apicomplexa-enriched (kinesin-X3 and kinesin-X4), and which lack genes for three classical kinesins (kinesin-1, -2 and -3) normally important in intracellular transport (5, 16).

The expression and subcellular location of each *Plasmodium* kinesin provides important information about their potential role. Kinesin-13 is the most widely expressed of these motors in all proliferative and invasive stages, with diverse cytoplasmic locations including axonemes in male gametocytes and at the apical end of the differentiating ookinete in addition to its association with the nuclear spindle apparatus. A similar diverse set of kinesin-13 locations has been reported in other eukaryotes (35-37), highlighting its importance for various MT-associated biological processes in *Plasmodium spp.*

The cytoplasmic location of three male gametocyte-specific kinesins (kinesin-8B, -15 and -X4) and kinesin-13, suggests their role in rapid axoneme assembly and flagellum formation in *Plasmodium spp*. The axonemes are assembled directly in the male gametocyte cytoplasm - there is thus no requirement for transport of building materials by the intraflagellar transport (IFT) mechanisms common in many other eukaryotes (38-40). Consistently, the IFT transport-associated kinesin-2 is absent from *Plasmodium*, further reinforcing the operation of non-canonical axoneme assembly mechanisms. In good agreement with our findings, a previous *P. berghei* male gamete

proteome study, three kinesins (kinesin-8B, -13 and -15) were identified and proposed to have an important role in axoneme assembly (41). In a recent study on the regulation of *P. berghei* male gametogenesis, many of the identified phospho-regulated proteins had motor activity, and included most of the *Plasmodium* kinesins (42). The expression of six kinesins (kinesin-5, -8B, -8X, -13, -15, and -X4) in gametocytes and their location in either nucleus (kinesin-5 and -8X), cytoplasm (kinesin-8B, -15, and -X4) or both (kinesin-13) suggest the importance of these kinesins in male gametogenesis and thus parasite transmission.

Kinesin-X3 and kinesin-X4, which are largely Apicomplexa-specific, show an interesting location on ookinete and sporozoite surface pellicle (-X3) and axonemes during male gametogenesis (-X4), respectively. These kinesins seem to have evolved in Apicomplexa for different MT- based structures such as the axoneme of flagella and a cytoskeletal scaffold to establish and maintain cell polarity, shape, and motility. The absence of kinesin-X3 from the apical end highlights that it is not a part of the conoidal complex (11, 43). Kinesin-20 has a ring-like location at the junction between the protrusion and the main cell body of the developing ookinete, suggesting a role in formation of the IMC/sub-pellicular microtubule complex and defining the size and shape of the cell, and then disappears from the mature cell. *Plasmodium* Myosin F has a similar location in early stages of ookinete development (27) suggesting the existence of an actomyosin contractile ring that might be regulated by kinesin-20.

Genetic analysis revealed that most of the kinesins (8 out of 9) have their most important roles in transmission stages within the mosquito, where there are substantial changes in cell size, morphology, and invasive properties, which may be regulated by MTs and associated proteins. For example, the results of our ultrastructural analysis of *Δkinesin-20* parasites show that loss of this kinesin affects the development of ookinete shape and size. MT length, number and association with the IMC are crucial to determine the size, shape and motility of certain *Plasmodium spp.* stages (34). We show that kinesin-20 regulates the length and arrangement of subpellicular MTs of developing ookinetes. Subpellicular MTs along with IMC proteins maintain ookinete polarity and morphology in *Plasmodium spp.* (23). IMC1b-deficient ookinetes display abnormal cell shape and reduced gliding motility (44) similar to the properties of *Δkinesin-20,* and a similar phenotype was observed in a recent study showing that palmitoylation of IMC subcompartment proteins (ISPs) regulates the apical subpellicular MT network in ookinetes and affects their elongation (45). ISPs also maintain the polar location of guanylate cyclase beta (GCβ)/CDC50A complex at the IMC, essential for ookinete gliding (46). PPKL-deficient parasites also have a defective MT organisation and abnormal shaped ookinetes (47), but the *Δkinesin-20* phenotype is slightly different, with no defect in the apical ring, which serves as an MT organising centre for subpellicular MTs, and similar to what was found for phosphodiesterase-δ (*pdeδ*) deficient ookinetes, which lack this enzyme involved in cyclic GMP signaling (48). The kinesin-20GFP location suggests there is a ring-like structure at the junction of the protrusion and cell body, which defines the developing ookinete shape and diameter, while apical polarity guides ookinete size and differentiation. An actomyosin contractile ring is present in elongation of embryonic cells of *Ciona intestinalis*, a primitive chordate (49). The assembly and organization of an actomyosin contractile ring during cytokinesis is highly dynamic and contains, in addition to actin and myosin, other proteins that regulate actin nucleation, cross-linking and myosin activity (50, 51). In *Plasmodium spp.* and other members of Apicomplexa, a similar contractile ring has been reported as required for cytokinesis (52, 53) but an involvement in cell elongation is unknown. Kinesin-20 could

be a protein that regulates contractile ring function in cell elongation during ookinete development.

The in-depth structural analysis of *kinesin-13PTD* parasites reveals the importance of kinesin-13 in regulating MT organisation in sexual stages in the mosquito. Kinesin-13s are MT depolymerising kinesins, playing essential roles in spindle MT dynamics, kinetochore-MT attachment, and chromosome segregation (35-37). *Plasmodium falciparum* kinesin-13 has also been shown to exhibit MT depolymerisation activity *in vitro* (54). Kinesin-13 homologs are present in most eukaryotes possessing cilia or flagella (55) and regulate the length of these structures (56-58). The knockdown of *P. berghei* kinesin-13 resulted in defects in the organisation of both spindle and axonemal MTs, thus arresting nuclear division and axoneme assembly during male gametogenesis. A similar phenotype was observed for the kinesin-8B gene knockout, which shows defective basal body formation and axoneme assembly during male gametogenesis, but nuclear division was normal (18). Knockout of the gene for another basal body protein, SAS6, resulted in a similar phenotype with defective basal body formation and axoneme assembly but no effect on nuclear division (59). Disruption of the gene for PF16, an armadillo-repeat protein of *Plasmodium spp.,* produces a similar phenotype, with an effect on axonemal central MT assembly and male gamete motility and fertility (60). We found a cdc2-related kinase (CRK5) that is important for nuclear spindle formation but has no effect on axoneme assembly during male gametogenesis (61). Previous studies have shown a similar phenotype for CDPK4 and MAP2 gene disruptions, where either the early or late stages of exflagellation are impaired but axoneme assembly is not (20, 62-64). In another primitive eukaryote, *Giardia intestinalis*, kinesin-13 regulates MT dynamics during both flagellar assembly and nuclear division (65).

Kinesin-13 has an additional role during zygote to ookinete transformation as shown by kinesin-13PTD parasites producing retorts. Ultrastructure analysis of these retorts revealed a loss of polarity and disorganisation of the subpellicular MTs, consistent with the additional polar localization of kinesin-13GFP in zygotes and during ookinete development. This phenotype of kinesin-13 depletion is different from that of the *Δkinesin-20*, where apical polarity was not affected. A similar phenotype has been observed following knockdown of two *P. berghei* phosphatases, PPKL and PP1, where apical polarity was lost, affecting ookinete differentiation (47, 66).

Global transcriptomic analysis supports the idea of a defect in spindle formation and axoneme assembly during male gametogenesis in kinesin-13 depleted parasites, as the expression of several genes involved in chromosome segregation, axoneme biogenesis, IMC/glideosome formation and other biological processes were modulated in *kinesin-13PTD* parasites. For example, differentially expressed genes like CRK5, SRPK and CDPK4 are involved in mitotic spindle formation during male gametogenesis (20, 62, 63). Similarly, kinesin-8B, kinesin-X4, dynein and radial spoke proteins are involved in axoneme assembly, male gamete formation and fertility (18, 41, 67). The compensatory expression of these genes is high in kinesin-13 depleted gametocytes suggesting their role in the same pathway during male gametogenesis, but it is insufficient to rescue the phenotype. Differential expression of genes like IMCs and GAPs indicates the additional role of kinesin-13 in glideosome formation and motility. Most of these changes in gene expression are obvious at 15 min post activation of gametocytes prior to gamete formation and fertilization. Translation repression in *Plasmodium spp*. is released after fertilization, allowing the stored transcripts in female gametocytes to be translated to form proteins essential for zygote development and ookinete invasion (28). Differential expression, mainly upregulation of these genes in *kinesin-13PTD* parasites, suggests a

compensatory role during male gametogenesis and ookinete formation. Overall, these global transcriptomic data for *kinesin-13PTD* parasites are consistent with the profound phenotypic changes observed during male gametogenesis and ookinete formation.

In conclusion, the nine *P. berghei* kinesins show a diverse pattern of expression and subcellular location at various stages of the parasite life cycle. Genetic and phenotypic analyses indicate that most kinesins have their most important roles in mosquito stages, except kinesin-13 which is also essential for asexual blood stages**.** Kinesin-20 and kinesin-13 have roles in MT dynamics during proliferation, polarity formation, and transmission of the parasite. It will be interesting in the future to look for the interacting partners of these kinesins and understand their mechanisms of action during these biological processes. This comprehensive study provides knowledge and understanding of the important roles of kinesins in various cellular processes at different stages of the life cycle of this evolutionarily divergent eukaryotic pathogen. This information may be useful to exploit kinesins as potential targets for new therapeutic interventions against malaria.

Materials and Methods

Ethics statement

The animal work passed an ethical review process and was approved by the United Kingdom Home Office. Work was carried out under UK Home Office Project Licenses (30/3248 and PDD2D5182) in accordance with the UK 'Animals (Scientific Procedures) Act 1986'. Six- to eight-week-old female CD1 outbred mice from Charles River laboratories were used for all experiments.

Generation of transgenic parasites and genotype analyses

To observe the location of kinesin proteins, the C-terminus was tagged with green fluorescent protein (GFP) sequence by single crossover homologous recombination at the 3' end of the gene. To generate the GFP-tag line, a region of these genes downstream of the ATG start codon was amplified, ligated to p277 vector, and transfected as described previously (47). The p277 vector contains the human *dhfr* cassette, conveying resistance to pyrimethamine. A schematic representation of the endogenous gene locus, the constructs and the recombined gene locus can be found in **S1A Fig.** For the parasites expressing a C-terminal GFP-tagged protein, diagnostic PCR was used with primer 1 (Int primer) and primer 3 (ol492) to confirm integration of the GFP targeting construct **(S1B Fig).** A list of primers used to amplify these genes can be found in **S2 Table**.

The gene-deletion targeting vectors for kinesin genes *were* constructed using the pBS-DHFR plasmid, which contains polylinker sites flanking a *Toxoplasma gondii dhfr/ts* expression cassette conferring resistance to pyrimethamine, as described previously (20). The 5′ upstream sequences from genomic DNA of kinesin genes were amplified and inserted into *Apa*I and *Hin*dIII restriction sites upstream of the *dhfr/ts* cassette of pBS-DHFR. The DNA fragments amplified from the 3′ flanking region of kinesin genes *w*ere then inserted downstream of the *dhfr/ts* cassette using *Eco*RI and *Xba*I restriction sites. The linear targeting sequence was released using *Apa*I/*Xba*I. A schematic representation of the endogenous *kinesin* loci, the constructs and the recombined *kinesin* loci can be found in **S3 Fig**. The primers used to generate the mutant parasite lines can be found in **S2 Table**. A diagnostic PCR was used with primer 1 (Int primer) and primer 2 (ol248) to confirm integration of the targeting construct, and primer 3 (KO1) and primer 4 (KO2) were used to confirm deletion of the *kinesin* genes **(S3 Fig, S2 Table)**.

To study the function of kinesin-13, we used two conditional knock-down systems; an auxin inducible degron (kinesin13AID) system and a promoter exchange/trap using double homologous recombination (kinesin-13PTD). For the generation of transgenic kinesin-13AID/HA line, library clone PbG01-2471h08 from the PlasmoGEM repository (http://plasmogem.sanger.ac.uk/) was used. Sequential recombineering and gateway steps were performed as previously described (68, 69). Insertion of the GW cassette following gateway reaction was confirmed using primer pairs GW1 x *kinesin-13* QCR1 and GW2 x *kinesin-13* QCR2. The modified library inserts were then released from the plasmid backbone using NotI. The kinesin-13-AID/HA targeting vector was transfected into the 615-parasite line and conditional degradation of kinesin-13-AID/HA in the non-clonal line was performed as described previously (61). A schematic representation of the endogenous *kinesin-13* locus, the constructs and the recombined *kinesin-13* locus can be found in **S7A Fig.** A diagnostic PCR was performed for *kinesin-13* gene knockdown parasites as outlined in **S7A Fig.**. Primer pairs *Kinesin-13*QCR1/GW1, and

Kinesin-13 QCR2/GW2 were used to determine successful integration of the targeting construct at the 3' end of the gene **(S7B Fig)**.

The conditional knockdown construct kinesin-13PTD was derived from P_{clag} (pSS367) where *kinesin-13* was placed under the control of the *clag* gene (PBANKA_083630) promoter, as described previously (31). A schematic representation of the endogenous *kinesin-13* locus, the constructs and the recombined *kinesin-13* locus can be found in **S7D Fig**. A diagnostic PCR was performed for *kinesin-13* gene knockdown parasites as outlined in **S7D Fig**. Primer 1 (5'-intPTD50) and Primer 2 (5'-intPTD) were used to determine successful integration of the targeting construct at the 5' end of the gene. Primer 3 (3'-intPTclag) and Primer 4 (3'-intPTD50) were used to determine successful integration for the 3' end of the gene locus **(S7E Fig)**. All the primer sequences can be found in **S2Table**. *P. berghei* ANKA line 2.34 (for GFP-tagging) or ANKA line 507cl1 expressing GFP (for the gene deletion and knockdown construct) parasites were transfected by electroporation (70).

Parasite phenotype analyses

Blood containing approximately 50,000 parasites of the kinesin knockout/knockdown lines was injected intraperitoneally (i.p) into mice to initiate infection. Asexual stages and gametocyte production were monitored by microscopy on Giemsa-stained thin smears. Four to five days post infection, exflagellation and ookinete conversion were examined as described previously (47) with a Zeiss AxioImager M2 microscope (Carl Zeiss, Inc) fitted with an AxioCam ICc1 digital camera. To analyse mosquito transmission, 30–50 *Anopheles stephensi* SD 500 mosquitoes were allowed to feed for 20 min on anaesthetized, infected mice whose asexual parasitaemia had reached 15% and were carrying comparable numbers of gametocytes as determined on Giemsa stained blood films. To assess mid-gut infection, approximately 15 guts were dissected from mosquitoes on day-7 and -14 post feeding and oocysts were counted using a 63x oil immersion objective. On day 21 post-feeding, another 20 mosquitoes were dissected, and their guts and salivary glands crushed separately in a loosely fitting homogenizer to release sporozoites, which were then quantified using a haemocytometer or used for imaging. Mosquito bite back experiments were performed 21 days post-feeding using naive mice, and blood smears were examined after 3-4 days.

Purification of schizonts, gametocytes and ookinetes

Blood cells obtained from infected mice (day 4 post infection) were cultured for 8 h and 24 h at 37˚C (with rotation at 100 rpm) and schizonts were purified on a 60% v/v NycoDenz (in PBS) gradient, (NycoDenz stock solution: 27.6% w/v NycoDenz in 5 mM Tris-HCl, pH 7.20, 3 mM KCl, 0.3 mM EDTA).

The purification of gametocytes was achieved by injecting parasites into phenylhydrazine treated mice (71) and enriched by sulfadiazine treatment after 2 days of infection. The blood was collected on day 4 after infection and gametocyte-infected cells were purified on a 48% v/v NycoDenz (in PBS) gradient (NycoDenz stock solution: 27.6% w/v NycoDenz in 5 mM Tris-HCl, pH 7.20, 3 mM KCl, 0.3 mM EDTA). The gametocytes were harvested from the interface and activated.

Blood cells obtained from infected mice (day 4-5 post infection) with high gametocytemia (>20%) were cultured for 24 h in ookinete medium containing xanthurenic acid at 20 °C. The ookinetes were pelleted at 1900 rpm (500 *g*), the supernatant was discarded, and the cells were resuspended in 8 ml ookinete medium. Five µl of magnetic beads coated with 13.1 antibody (anti-P28 of ookinete) were added and incubated for 10 min at RT with continuous mixing. The tubes were placed on the magnet (Dyna rack) for 2 min and

supernatant was transferred into new tubes. The beads with bound ookinetes were washed with 2 ml of ookinete medium and used for imaging or electron microscopy.

Immunoprecipitation and mass spectrometry

Male gametocytes of kinesin-GFP parasites were used 1-2 min post activation to prepare cell lysates. WT-ANKA and non-kinesin proteins tagged with GFP were used as negative controls. Immunoprecipitation was performed using the protein lysates and a GFP-Trap_A Kit (Chromotek) following the manufacturer's instructions. Briefly, the lysates were incubated for 2h with GFP-Trap_A beads at 4º C with continuous rotation. Unbound proteins were washed, and proteins bound to the GFP-Trap_A beads were digested using trypsin and the peptides were analysed by liquid chromatography–tandem mass spectrometry. Mascot (http://www.matrixscience.com/) and MaxQuant (https://www.maxquant.org/) search engines were used for mass spectrometry data analysis. The PlasmoDB database was used for protein annotation. Peptide and proteins having minimum threshold of 95% were used for further proteomic analysis.

Live cell imaging

To examine kinesin-GFP expression during erythrocyte stages, parasites growing in schizont culture medium were used for imaging at different stages (ring, trophozoite, schizont and merozoite) of development. Purified gametocytes were examined for GFP expression and cellular location at different time points (0, 1-15 min) after activation in ookinete medium (16). Zygote and ookinete stages were analyzed throughout 24 h of culture. Oocysts and sporozoites were imaged using infected mosquito guts. Images were captured using a 63x oil immersion objective on a Zeiss Axio Imager M2 microscope fitted with an AxioCam ICc1 digital camera.

Generation of dual tagged parasite lines

The kinesin-GFP (kinesin-5, -8X, -13 and -X4) parasites were mixed with NDC80-cherry and kinesin8B-cherry parasites in equal numbers and injected into mice. Mosquitoes were fed on mice 4 to 5 days after infection when gametocytemia was high. These mosquitoes were checked for oocyst development and sporozoite formation at day 14 and day 21 after feeding. Infected mosquitoes were then allowed to feed on naïve mice and after 4 - 5 days the mice were examined for blood stage parasitaemia by microscopy with Giemsa-stained blood smears. In this way, some parasites expressed both kinesin-GFP and NDC80-cherry; and kinesin-GFP and kinesin-8B-cherry in the resultant gametocytes, and these were purified and fluorescence microscopy images were collected as described above.

Ookinete and sporozoite motility assays

Sporozoites were isolated from the salivary glands of mosquitoes infected with WTGFP and Δ*kinesin-20* parasites 21 days post infection. Isolated sporozoites in RPMI 1640 containing 3% bovine serum albumin (Fisher Scientific) were pelleted (5 min, 5,000 rpm, 4°C) and used for motility assay. The assay using Matrigel was performed as described previously (17, 26). A small volume (20 µl) of sporozoites, isolated as above for WT-GFP and Δ*kinesin-20* parasites, were mixed with Matrigel (Corning). The mixture (6 µl) was transferred onto a microscope slide with a cover slip and sealed with nail polish. After identifying a field containing sporozoites, time-lapse videos (one frame every 2 s for 100 cycles) were taken using the differential interference contrast settings with a 63× objective lens on a Zeiss AxioImager M2 microscope fitted with an AxioCam ICc1 digital camera and analysed with the AxioVision 4.8.2 software.

For ookinete motility, 24 h ookinete cultures were added to an equal volume of Matrigel on ice, mixed thoroughly, dropped onto a slide, covered with a cover slip, and sealed with nail polish. The Matrigel was then allowed to set at 20°C for 30 min. After identifying a field containing ookinetes, time-lapse videos were taken (one frame every 5 s for 100 cycles).

Fixed immunofluorescence assay

The kinesin-GFP gametocytes were purified, activated in ookinete medium, fixed with 4% paraformaldehyde (PFA, Sigma) diluted in microtubule stabilising buffer (MTSB) for 10-15 min and added to poly-L-lysine coated slides. Immunocytochemistry was performed using primary GFP-specific rabbit monoclonal antibody (mAb) (Invitrogen-A1122; used at 1:250) and primary mouse anti-α tubulin mAb (Sigma-T9026; used at 1:1000). Secondary antibodies were Alexa 488 conjugated anti-mouse IgG (Invitrogen-A11004) and Alexa 568 conjugated anti-rabbit IgG (Invitrogen-A11034) (used at 1 in 1000). The slides were then mounted in Vectashield 19 with DAPI (Vector Labs) for fluorescence microscopy. Parasites were visualised on a Zeiss AxioImager M2 microscope fitted with an AxioCam ICc1 digital camera.

Ultrastructure expansion microscopy (U-ExM)

Purified gametocytes were activated for 4-5 min and 15 min; activation was stopped by adding 1X ice cold PBS. Activated gametocytes and mature ookinetes were sedimented onto 12 mm round Poly-D-Lysine (A3890401, Gibco) coated coverslips for 10 min (gametocyte procedure was performed on ice), fixed in methanol at −20°C for 7 min, and then prepared for U-ExM as described previously (43, 72). Immuno-labelling was performed using primary antibody against α-tubulin and β-tubulin (1:200 dilution, source: Geneva antibody facility) and secondary antibody anti-guinea pig Alexa 488 (1:400 dilution, source: ThermoFisher). Images were acquired on a Leica TCS SP8 microscope, image analysis was performed using Fiji-Image J and Leica Application Suite X (LAS X) software.

Electron microscopy

Gametocytes activated for 6 min and 15 min and ookinetes were fixed in 4% glutaraldehyde in 0.1 M phosphate buffer and processed for electron microscopy (73). Briefly, samples were post fixed in osmium tetroxide, treated *en bloc* with uranyl acetate, dehydrated and embedded in Spurr's epoxy resin. Thin sections were stained with uranyl acetate and lead citrate prior to examination in a JEOL JEM-1400 electron microscope (JEOL Ltd, UK).

RNA isolation and quantitative Real Time PCR (qRT-PCR) analyses

RNA was isolated from purified gametocytes using an RNA purification kit (Stratagene). cDNA was synthesized using an RNA-to-cDNA kit (Applied Biosystems). Gene expression was quantified from 80 ng of total RNA using SYBR green fast master mix kit (Applied Biosystems). All the primers were designed using primer3 (Primer-blast, NCBI). Analysis was conducted using an Applied Biosystems 7500 fast machine with the following cycling conditions: 95˚C for 20 s followed by 40 cycles of 95˚C for 3 s; 60˚C for 30 s. Three technical replicates and three biological replicates were performed for each assayed gene. The *hsp70* (PBANKA_081890) and *arginyl-t RNA synthetase* (PBANKA_143420) genes were used as endogenous control reference genes. The primers used for qPCR can be found in **S2 Table**.

RNA-seq analysis

Libraries were prepared from lyophilized total RNA, first by isolating mRNA using NEBNext Poly(A) mRNA Magnetic Isolation Module (NEB), then using NEBNext Ultra Directional RNA Library Prep Kit (NEB) according to the manufacturer's instructions. Libraries were amplified for a total of 12 PCR cycles (12 cycles of [15 s at 98°C, 30 s at 55°C, 30 s at 62°C]) using the KAPA HiFi HotStart Ready Mix (KAPA Biosystems). Libraries were sequenced using a NovaSeq 6000 DNA sequencer (Illumina), producing paired-end 100-bp reads.

FastQC (https://www.bioinformatics.babraham.ac.uk/projects/fastqc/), was used to analyse raw read quality, and based on this information, the first 11 bp of each read and any adapter sequences were removed using Trimmomatic (http://www.usadellab.org/cms/?page=trimmomatic). Bases were trimmed from reads using Sickle with a Phred quality threshold of 25 (https://github.com/najoshi/sickle). The resulting reads were mapped against the *P. berghei* ANKA genome (v36) using HISAT2 (version 2-2.1.0), using default parameters. Uniquely mapped, properly paired reads with mapping quality 40 or higher were retained using SAMtools (http://samtools.sourceforge.net/). Genome browser tracks were generated and viewed using the Integrative Genomic Viewer (IGV) (Broad Institute). Raw read counts were determined for each gene in the *P. berghei* genome using BedTools (https://bedtools.readthedocs.io/en/latest/#) to intersect the aligned reads with the genome annotation. Differential expression analysis was done by use of R package DESeq2 to call up- and down-regulated genes with an adjusted P-value cutoff of 0.05. Gene ontology enrichment was done using R package topGO (https://bioconductor.org/packages/release/bioc/html/topGO.html) with the weight01 algorithm.

ChIP-seq analysis

Gametocytes for kinesin-5GFP, kinesin-8XGFP, and NDC80GFP (as a positive control) parasites were harvested and the pellets were resuspended in 500 µl of Hi-C lysis buffer (25 mM Tris-HCl, pH 8.0, 10 mM NaCl, 2 mM AESBF, 1% NP-40, protease inhibitors). After incubation for 10 min at room temperature (RT), the resuspended pellets were homogenized by passing through a 26.5 gauge needle/syringe 15 times and cross-linked by adding formaldehyde (1.25% final concentration) for 25 min at RT with continuous mixing. Crosslinking was stopped by adding glycine to a final concentration of 150 mM and incubating for 15 min at RT with continuous mixing. The sample was centrifuged for 5 min at 2,500 x g (~5,000 rpm) at 4°C, the pellet washed once with 500 µl ice-cold wash buffer (50 mM Tris-HCl, pH 8.0, 50 mM NaCl, 1 mM EDTA, 2 mM AESBF, protease inhibitors) and the pellet stored at -80°C for ChIP seq analysis. The crosslinked parasite pellets were resuspended in 1 mL of nuclear extraction buffer (10 mM HEPES, 10 mM KCl, 0.1 mM EDTA, 0.1 mM EGTA, 1 mM DTT, 0.5 mM AEBSF, 1X protease inhibitor tablet), post 30 min incubation on ice, 0.25% Igepal-CA-630 was added and homogenized by passing through a 26G x ½ needle. The nuclear pellet extracted through 5000 rpm centrifugation, was resuspended in 130 µl of shearing buffer (0.1% SDS, 1 mM EDTA, 10 mM Tris-HCl pH 7.5, 1X protease inhibitor tablet), and transferred to a 130 µl Covaris sonication microtube. The sample was then sonicated using a Covaris S220 Ultrasonicator for 8 min (Duty cycle: 5%, Intensity peak power: 140, Cycles per burst: 200, Bath temperature: 6°C). The sample was transferred to ChIP dilution buffer (30 mM Tris-HCl pH 8, 3 mM EDTA, 0.1% SDS, 30 mM NaCl, 1.8% Triton X-100, 1X protease inhibitor tablet, 1X phosphatase inhibitor tablet) and centrifuged for 10 min at 13,000 rpm at 4°C, retaining the supernatant. For each sample, 13 µl of protein A

agarose/salmon sperm DNA beads were washed three times with 500 µl ChIP dilution buffer (without inhibitors) by centrifuging for 1 min at 1000 rpm at room temperature, then buffer was removed. For pre-clearing, the diluted chromatin samples were added to the beads and incubated for 1 hour at 4°C with rotation, then pelleted by centrifugation for 1 min at 1000 rpm. Before adding antibody, ~10% of one kin-8XGFP sample was taken as input. Supernatant was removed into a LoBind tube carefully so as not to remove any beads and 2 µg of anti-GFP antibody (Abcam ab290, anti-rabbit) were added to the sample and incubated overnight at 4°C with rotation. For one kinesin-8XGFP sample, IgG antibody (ab37415) was added instead as a negative control. Per sample, 25 µl of protein A agarose/salmon sperm DNA beads were washed with ChIP dilution buffer (no inhibitors), blocked with 1 mg/mL BSA for 1 hour at 4°C, then washed three more times with buffer. 25 µl of washed and blocked beads were added to the sample and incubated for 1 hour at 4°C with continuous mixing to collect the antibody/protein complex. Beads were pelleted by centrifugation for 1 min at 1000 rpm at 4°C. The bead/antibody/protein complex was then washed with rotation using 1 mL of each buffers twice; low salt immune complex wash buffer (1% SDS, 1% Triton X-100, 2 mM EDTA, 20 mM Tris-HCl pH 8, 150 mM NaCl), high salt immune complex wash buffer (1% SDS, 1% Triton X-100, 2 mM EDTA, 20 mM Tris-HCl pH 8, 500 mM NaCl), high salt immune complex wash buffer (1% SDS, 1% Triton X-100, 2 mM EDTA, 20 mM Tris-HCl pH 8, 500 mM NaCl), TE wash buffer (10 mM Tris-HCl pH 8, 1 mM EDTA) and eluted from antibody by adding 250 µl of freshly prepared elution buffer (1% SDS, 0.1 M sodium bicarbonate). We added 5 M NaCl to the elution and cross-linking was reversed by heating at 45°C overnight followed by addition of 15 µl of 20 mg/mL RNAase A with 30 min incubation at 37°C. After this, 10 µl 0.5 M EDTA, 20 µl 1 M Tris-HCl pH 7.5, and 2 µl 20 mg/mL proteinase K were added to the elution and incubated for 2 hours at 45°C. DNA was recovered by phenol/chloroform extraction and ethanol precipitation, using a phenol/chloroform/isoamyl alcohol (25:24:1) mixture twice and chloroform once, then adding 1/10 volume of 3 M sodium acetate pH 5.2, 2 volumes of 100% ethanol, and 1/1000 volume of 20 mg/mL glycogen. Precipitation was allowed to occur overnight at -20°C. Samples were centrifuged at 13,000 rpm for 30 min at 4°C, then washed with fresh 80% ethanol, and centrifuged again for 15 min with the same settings. Pellet was air-dried and resuspended in 50 µl nuclease-free water. DNA was purified using Agencourt AMPure XP beads. Libraries were then prepared from this DNA using a KAPA library preparation kit (KK8230) and sequenced on a NovaSeq 6000 machine. FastQC (https://www.bioinformatics.babraham.ac.uk/projects/fastqc/), was used to analyze raw read quality. Any adapter sequences were removed using Trimmomatic (http://www.usadellab.org/cms/?page=trimmomatic). Bases with Phred quality scores below 25 were trimmed using Sickle (https://github.com/najoshi/sickle). The resulting reads were mapped against the *P. berghei* ANKA genome (v36) using Bowtie2 (version 2.3.4.1). Using Samtools, only properly paired reads with mapping quality 40 or higher were retained and reads marked as PCR duplicates were removed by PicardTools MarkDuplicates (Broad Institute). Genome-wide read counts per nucleotide were normalized by dividing millions of mapped reads for each sample (for all samples including input) and subtracting input read counts from the ChIP and IgG counts. From these normalized counts, genome browser tracks were generated and viewed using the Integrative Genomic Viewer (IGV).

Statistical analysis

All statistical analyses were performed using GraphPad Prism 7 (GraphPad Software). For qRT-PCR, an unpaired t-test was used to examine significant differences between wild-type and mutant strains.

Acknowledgments

We wish to thank Julie Rodgers for helping to maintain the insectary and other technical works.

Funding: This work was supported by: MRC UK (G0900109, G0900278, MR/K011782/1) and BBSRC (BB/N017609/1) to RT; the BBSRC (BB/N017609/1) to MZ; the Francis Crick Institute (FC001097), the Cancer Research UK (FC001097), the UK Medical Research Council (FC001097), and the Wellcome Trust (FC001097) to AAH; the NIH/NIAID (R01 AI136511) and the University of California, Riverside (NIFA-Hatch-225935) to KGLR; the Swiss National Science Foundation project grant (31003A_179321) to MB and BBSRC (BB/N018176/1) to CAM. This research was funded in whole, or in part, by the Wellcome Trust [FC001097]. For the purpose of Open Access, the author has applied a CC BY public copyright licence to any Author Accepted Manuscript version arising from this submission.

Author contributions:

Conceptualization: RT
Methodology: MZ, DB, RT, RR, SA, ZC, DJPF
Investigation: MZ, DB, RT, RR, SA, ZC, DJPF
Visualization: MZ, RT, RR, SA, DJPF
Supervision: RT, AAH, KGLR, CAM, MB
Writing—original draft: RT, MZ
Writing—review & editing: RT, MZ, AAH, KGLR, CAM, MB, DJPF

Competing interests: All other authors declare they have no competing interests.

Data and materials availability: Sequence reads for ChIP-seq and RNA-seq have been deposited in the NCBI Sequence Read Archive with accession number: PRJNA731497. All other data are available in the main text or the supplementary materials.

References

1. Verhey KJ, Hammond JW. Traffic control: regulation of kinesin motors. Nat Rev Mol Cell Biol. 2009;10(11):765-77.
2. Konjikusic MJ, Gray RS, Wallingford JB. The developmental biology of kinesins. Dev Biol. 2021;469:26-36.
3. Hirokawa N, Tanaka Y. Kinesin superfamily proteins (KIFs): Various functions and their relevance for important phenomena in life and diseases. Exp Cell Res. 2015;334(1):16-25.
4. Yount AL, Zong H, Walczak CE. Regulatory mechanisms that control mitotic kinesins. Exp Cell Res. 2015;334(1):70-7.
5. Wickstead B, Gull K, Richards TA. Patterns of kinesin evolution reveal a complex ancestral eukaryote with a multifunctional cytoskeleton. BMC Evol Biol. 2010;10:110.

6. Vicente JJ, Wordeman L. Mitosis, microtubule dynamics and the evolution of kinesins. Exp Cell Res. 2015;334(1):61-9.
7. Wickstead B, Gull K. The evolution of the cytoskeleton. J Cell Biol. 2011;194(4):513-25.
8. Zeeshan M, Pandey R, Ferguson DJP, Tromer EC, Markus R, Abel S, et al. Real-time dynamics of Plasmodium NDC80 reveals unusual modes of chromosome segregation during parasite proliferation. J Cell Sci. 2020;134(5).
9. Sinden RE. Mitosis and meiosis in malarial parasites. Acta Leiden. 1991;60(1):19-27.
10. Sinden RE, Canning EU, Bray RS, Smalley ME. Gametocyte and gamete development in Plasmodium falciparum. Proc R Soc Lond B Biol Sci. 1978;201(1145):375-99.
11. Koreny L, Zeeshan M, Barylyuk K, Tromer EC, van Hooff JJE, Brady D, et al. Molecular characterization of the conoid complex in Toxoplasma reveals its conservation in all apicomplexans, including Plasmodium species. PLoS Biol. 2021;19(3):e3001081.
12. Janse CJ, Mons B, Rouwenhorst RJ, Van der Klooster PF, Overdulve JP, Van der Kaay HJ. In vitro formation of ookinetes and functional maturity of Plasmodium berghei gametocytes. Parasitology. 1985;91 (Pt 1):19-29.
13. Sinden RE, Strong K. An ultrastructural study of the sporogonic development of Plasmodium falciparum in Anopheles gambiae. Trans R Soc Trop Med Hyg. 1978;72(5):477-91.
14. Schrevel J, Asfaux-Foucher G, Bafort JM. [Ultrastructural study of multiple mitoses during sporogony of Plasmodium b. berghei]. J Ultrastruct Res. 1977;59(3):332-50.
15. Graumans W, Jacobs E, Bousema T, Sinnis P. When Is a Plasmodium-Infected Mosquito an Infectious Mosquito? Trends Parasitol. 2020;36(8):705-16.
16. Zeeshan M, Shilliday F, Liu T, Abel S, Mourier T, Ferguson DJP, et al. Plasmodium kinesin-8X associates with mitotic spindles and is essential for oocyst development during parasite proliferation and transmission. PLoS Pathog. 2019;15(10):e1008048.
17. Zeeshan M, Brady D, Stanway RR, Moores CA, Holder AA, Tewari R. Plasmodium berghei Kinesin-5 Associates With the Spindle Apparatus During Cell Division and Is Important for Efficient Production of Infectious Sporozoites. Front Cell Infect Microbiol. 2020;10:583812.
18. Zeeshan M, Ferguson DJ, Abel S, Burrrell A, Rea E, Brady D, et al. Kinesin-8B controls basal body function and flagellum formation and is key to malaria transmission. Life Sci Alliance. 2019;2(4).
19. Depoix D, Marques SR, Ferguson DJ, Chaouch S, Duguet T, Sinden RE, et al. Vital role for Plasmodium berghei Kinesin8B in axoneme assembly during male gamete formation and mosquito transmission. Cell Microbiol. 2020;22(3):e13121.
20. Tewari R, Straschil U, Bateman A, Bohme U, Cherevach I, Gong P, et al. The systematic functional analysis of Plasmodium protein kinases identifies essential regulators of mosquito transmission. Cell Host Microbe. 2010;8(4):377-87.
21. Bushell E, Gomes AR, Sanderson T, Anar B, Girling G, Herd C, et al. Functional Profiling of a Plasmodium Genome Reveals an Abundance of Essential Genes. Cell. 2017;170(2):260-72 e8.
22. Gould SB, Tham WH, Cowman AF, McFadden GI, Waller RF. Alveolins, a new family of cortical proteins that define the protist infrakingdom Alveolata. Mol Biol Evol. 2008;25(6):1219-30.

23. Kono M, Prusty D, Parkinson J, Gilberger TW. The apicomplexan inner membrane complex. Front Biosci (Landmark Ed). 2013;18:982-92.
24. Iwanaga S, Kato T, Kaneko I, Yuda M. Centromere plasmid: a new genetic tool for the study of Plasmodium falciparum. PLoS One. 2012;7(3):e33326.
25. Pandey R, Abel S, Boucher M, Wall RJ, Zeeshan M, Rea E, et al. Plasmodium Condensin Core Subunits SMC2/SMC4 Mediate Atypical Mitosis and Are Essential for Parasite Proliferation and Transmission. Cell Rep. 2020;30(6):1883-97 e6.
26. Volkmann K, Pfander C, Burstroem C, Ahras M, Goulding D, Rayner JC, et al. The alveolin IMC1h is required for normal ookinete and sporozoite motility behaviour and host colonisation in Plasmodium berghei. PLoS One. 2012;7(7):e41409.
27. Wall RJ, Zeeshan M, Katris NJ, Limenitakis R, Rea E, Stock J, et al. Systematic analysis of Plasmodium myosins reveals differential expression, localisation, and function in invasive and proliferative parasite stages. Cell Microbiol. 2019;21(10):e13082.
28. Mair GR, Braks JA, Garver LS, Wiegant JC, Hall N, Dirks RW, et al. Regulation of sexual development of Plasmodium by translational repression. Science. 2006;313(5787):667-9.
29. Reid AJ, Talman AM, Bennett HM, Gomes AR, Sanders MJ, Illingworth CJR, et al. Single-cell RNA-seq reveals hidden transcriptional variation in malaria parasites. Elife. 2018;7.
30. Philip N, Waters AP. Conditional Degradation of Plasmodium Calcineurin Reveals Functions in Parasite Colonization of both Host and Vector. Cell Host Microbe. 2015;18(1):122-31.
31. Sebastian S, Brochet M, Collins MO, Schwach F, Jones ML, Goulding D, et al. A Plasmodium calcium-dependent protein kinase controls zygote development and transmission by translationally activating repressed mRNAs. Cell Host Microbe. 2012;12(1):9-19.
32. Gubbels MJ, Keroack CD, Dangoudoubiyam S, Worliczek HL, Paul AS, Bauwens C, et al. Fussing About Fission: Defining Variety Among Mainstream and Exotic Apicomplexan Cell Division Modes. Front Cell Infect Microbiol. 2020;10:269.
33. Morrissette NS, Sibley LD. Cytoskeleton of apicomplexan parasites. Microbiol Mol Biol Rev. 2002;66(1):21-38; table of contents.
34. Spreng B, Fleckenstein H, Kubler P, Di Biagio C, Benz M, Patra P, et al. Microtubule number and length determine cellular shape and function in Plasmodium. EMBO J. 2019;38(15):e100984.
35. Ems-McClung SC, Walczak CE. Kinesin-13s in mitosis: Key players in the spatial and temporal organization of spindle microtubules. Semin Cell Dev Biol. 2010;21(3):276-82.
36. Ali A, Veeranki SN, Chinchole A, Tyagi S. MLL/WDR5 Complex Regulates Kif2A Localization to Ensure Chromosome Congression and Proper Spindle Assembly during Mitosis. Dev Cell. 2017;41(6):605-22 e7.
37. Manning AL, Ganem NJ, Bakhoum SF, Wagenbach M, Wordeman L, Compton DA. The kinesin-13 proteins Kif2a, Kif2b, and Kif2c/MCAK have distinct roles during mitosis in human cells. Mol Biol Cell. 2007;18(8):2970-9.
38. Briggs LJ, Davidge JA, Wickstead B, Ginger ML, Gull K. More than one way to build a flagellum: comparative genomics of parasitic protozoa. Curr Biol. 2004;14(15):R611-2.
39. Mirvis M, Stearns T, James Nelson W. Cilium structure, assembly, and disassembly regulated by the cytoskeleton. Biochem J. 2018;475(14):2329-53.
40. Sinden RE, Talman A, Marques SR, Wass MN, Sternberg MJ. The flagellum in malarial parasites. Curr Opin Microbiol. 2010;13(4):491-500.

41. Talman AM, Prieto JH, Marques S, Ubaida-Mohien C, Lawniczak M, Wass MN, et al. Proteomic analysis of the Plasmodium male gamete reveals the key role for glycolysis in flagellar motility. Malar J. 2014;13:315.
42. Invergo BM, Brochet M, Yu L, Choudhary J, Beltrao P, Billker O. Sub-minute Phosphoregulation of Cell Cycle Systems during Plasmodium Gamete Formation. Cell Rep. 2017;21(7):2017-29.
43. Bertiaux E, Balestra AC, Bournonville L, Louvel V, Maco B, Soldati-Favre D, et al. Expansion microscopy provides new insights into the cytoskeleton of malaria parasites including the conservation of a conoid. PLoS Biol. 2021;19(3):e3001020.
44. Tremp AZ, Khater EI, Dessens JT. IMC1b is a putative membrane skeleton protein involved in cell shape, mechanical strength, motility, and infectivity of malaria ookinetes. J Biol Chem. 2008;283(41):27604-11.
45. Wang X, Qian P, Cui H, Yao L, Yuan J. A protein palmitoylation cascade regulates microtubule cytoskeleton integrity in Plasmodium. EMBO J. 2020;39(13):e104168.
46. Gao H, Yang Z, Wang X, Qian P, Hong R, Chen X, et al. ISP1-Anchored Polarization of GCbeta/CDC50A Complex Initiates Malaria Ookinete Gliding Motility. Curr Biol. 2018;28(17):2763-76 e6.
47. Guttery DS, Poulin B, Ferguson DJ, Szoor B, Wickstead B, Carroll PL, et al. A unique protein phosphatase with kelch-like domains (PPKL) in Plasmodium modulates ookinete differentiation, motility and invasion. PLoS Pathog. 2012;8(9):e1002948.
48. Moon RW, Taylor CJ, Bex C, Schepers R, Goulding D, Janse CJ, et al. A cyclic GMP signalling module that regulates gliding motility in a malaria parasite. PLoS Pathog. 2009;5(9):e1000599.
49. Sehring IM, Dong B, Denker E, Bhattachan P, Deng W, Mathiesen BT, et al. An equatorial contractile mechanism drives cell elongation but not cell division. PLoS Biol. 2014;12(2):e1001781.
50. Vavylonis D, Wu JQ, Hao S, O'Shaughnessy B, Pollard TD. Assembly mechanism of the contractile ring for cytokinesis by fission yeast. Science. 2008;319(5859):97-100.
51. Mangione MC, Gould KL. Molecular form and function of the cytokinetic ring. J Cell Sci. 2019;132(12).
52. Hammarton TC. Who Needs a Contractile Actomyosin Ring? The Plethora of Alternative Ways to Divide a Protozoan Parasite. Front Cell Infect Microbiol. 2019;9:397.
53. Morano AA, Dvorin JD. The Ringleaders: Understanding the Apicomplexan Basal Complex Through Comparison to Established Contractile Ring Systems. Front Cell Infect Microbiol. 2021;11:656976.
54. Moores CA, Yu M, Guo J, Beraud C, Sakowicz R, Milligan RA. A mechanism for microtubule depolymerization by KinI kinesins. Mol Cell. 2002;9(4):903-9.
55. Wickstead B, Gull K. A "holistic" kinesin phylogeny reveals new kinesin families and predicts protein functions. Mol Biol Cell. 2006;17(4):1734-43.
56. Vasudevan KK, Jiang YY, Lechtreck KF, Kushida Y, Alford LM, Sale WS, et al. Kinesin-13 regulates the quantity and quality of tubulin inside cilia. Mol Biol Cell. 2015;26(3):478-94.
57. Chan KY, Ersfeld K. The role of the Kinesin-13 family protein TbKif13-2 in flagellar length control of Trypanosoma brucei. Mol Biochem Parasitol. 2010;174(2):137-40.
58. Piao T, Luo M, Wang L, Guo Y, Li D, Li P, et al. A microtubule depolymerizing kinesin functions during both flagellar disassembly and flagellar assembly in Chlamydomonas. Proc Natl Acad Sci U S A. 2009;106(12):4713-8.

59. Marques SR, Ramakrishnan C, Carzaniga R, Blagborough AM, Delves MJ, Talman AM, et al. An essential role of the basal body protein SAS-6 in Plasmodium male gamete development and malaria transmission. Cell Microbiol. 2015;17(2):191-206.
60. Straschil U, Talman AM, Ferguson DJ, Bunting KA, Xu Z, Bailes E, et al. The Armadillo repeat protein PF16 is essential for flagellar structure and function in Plasmodium male gametes. PLoS One. 2010;5(9):e12901.
61. Balestra AC, Zeeshan M, Rea E, Pasquarello C, Brusini L, Mourier T, et al. A divergent cyclin/cyclin-dependent kinase complex controls the atypical replication of a malaria parasite during gametogony and transmission. Elife. 2020;9.
62. Fang H, Klages N, Baechler B, Hillner E, Yu L, Pardo M, et al. Multiple short windows of calcium-dependent protein kinase 4 activity coordinate distinct cell cycle events during Plasmodium gametogenesis. Elife. 2017;6.
63. Rashpa R, Brochet M. Expansion microscopy of Plasmodium gametocytes reveals the molecular architecture of a bipartite microtubule organisation centre coordinating mitosis with axoneme assembly. PLoS Pathog. 2022;18(1):e1010223.
64. Tewari R, Dorin D, Moon R, Doerig C, Billker O. An atypical mitogen-activated protein kinase controls cytokinesis and flagellar motility during male gamete formation in a malaria parasite. Mol Microbiol. 2005;58(5):1253-63.
65. Dawson SC, Sagolla MS, Mancuso JJ, Woessner DJ, House SA, Fritz-Laylin L, et al. Kinesin-13 regulates flagellar, interphase, and mitotic microtubule dynamics in Giardia intestinalis. Eukaryot Cell. 2007;6(12):2354-64.
66. Zeeshan M, Pandey R, Subudhi AK, Ferguson DJP, Kaur G, Rashpa R, et al. Protein Phosphatase 1 regulates atypical mitotic and meiotic division in Plasmodium sexual stages. bioRxiv. 2021.
67. Andreadaki M, Pace T, Grasso F, Siden-Kiamos I, Mochi S, Picci L, et al. Plasmodium berghei Gamete Egress Protein is required for fertility of both genders. Microbiologyopen. 2020;9(7):e1038.
68. Pfander C, Anar B, Brochet M, Rayner JC, Billker O. Recombination-mediated genetic engineering of Plasmodium berghei DNA. Methods Mol Biol. 2013;923:127-38.
69. Pfander C, Anar B, Schwach F, Otto TD, Brochet M, Volkmann K, et al. A scalable pipeline for highly effective genetic modification of a malaria parasite. Nat Methods. 2011;8(12):1078-82.
70. Janse CJ, Franke-Fayard B, Mair GR, Ramesar J, Thiel C, Engelmann S, et al. High efficiency transfection of Plasmodium berghei facilitates novel selection procedures. Molecular and biochemical parasitology. 2006;145(1):60-70.
71. Beetsma AL, van de Wiel TJ, Sauerwein RW, Eling WM. Plasmodium berghei ANKA: purification of large numbers of infectious gametocytes. Exp Parasitol. 1998;88(1):69-72.
72. Gambarotto D, Hamel V, Guichard P. Ultrastructure expansion microscopy (U-ExM). Methods Cell Biol. 2021;161:57-81.
73. Ferguson DJ, Henriquez FL, Kirisits MJ, Muench SP, Prigge ST, Rice DW, et al. Maternal inheritance and stage-specific variation of the apicoplast in Toxoplasma gondii during development in the intermediate and definitive host. Eukaryot Cell. 2005;4(4):814-26.

Figure legends

Fig 1. Subcellular location and function of kinesins at various stages of the *Plasmodium berghei* life cycle. (A) Life cycle of *Plasmodium spp*. showing different

proliferative and invasive stages in host and vector. **(B)** Live cell imaging showing subcellular locations of representative kinesin-GFP proteins (green) during various stages of the *P. berghei* life cycle. DNA is stained with Hoechst dye (blue). Scale bar = 5 µm. Underlying images for different stages are provided in the supplementary figure S3. **(C)** A summary of expression and location of kinesins-GFP during different stages of *P. berghei* life cycle. **(D)** Summary of phenotypes resulting from deletion of different kinesin genes at various stages of life cycle. The phenotype was examined for asexual blood stage development (schizogony), exflagellation (male gamete formation), ookinete formation, oocyst number, oocyst size, sporozoite formation in oocyst, presence of salivary gland sporozoites and sporozoite transmission to vertebrate host. N/D = Not Determined.

Fig 2. Apicomplexa-enriched kinesins (kinesin-X3 and –X4) are located at the pellicle during ookinete differentiation and at axonemes in male gametogenesis, respectively, while nuclear kinesin (kinesin-8X) associates with the kinetochore at the centromere during male gamete formation. (A) Live cell imaging showing temporal location of kinesin-X3 (green) associated with pellicle formation (arrows) during zygote to ookinete transition (2-24 h after fertilization)**.** A cy3-conjugated antibody, 13.1, which recognizes the protein P28 on the surface of zygote and ookinete stages, was used to track these stages (red). DNA is stained with Hoechst dye (blue). Scale bar = 5 µm. **(B)** Live cell imaging shows the association of kinesin-X4 (green) with axoneme marker kinesin-8B (red) during male gametogenesis. Note in later stages, axonemes (arrows) are labelled with both markers. DNA is stained with Hoechst dye (blue). Mpa = min post activation. Scale bar = 5 µm. **(C)** Co-localization of Pbkinesin-8X (red) and α-tubulin (green) in activated male gametocytes, shown by indirect immunofluorescence assay. Scale bar = 5 µm. **(D)** Live cell imaging showing the dynamics of kinesin-8XGFP (green) along with kinetochore marker NDC80Cherry (red) during male gametogenesis**.** DNA is stained with Hoechst dye (blue); mpa = min post activation; Scale bar = 5 µm. A diagrammatic representation of spindle/spindle pole and kinetochore is shown in upper panels. **(E)** ChIP-seq analysis of kinesin-8X and NDC80 during gametocyte stage. Lines on top are division points between chromosomes and circles on the bottom indicate locations of centromeres.

Fig 3. Kinesin-20 makes a ring like structure at the base of developing ookinete and is important for zygote to ookinete transformation and subsequent motility. (A) Live cell imaging showing localization of kinesin-20GFP (green) in the female gametocyte, zygote and during ookinete transformation. Kinesin-20GFP accumulates at the neck of developing ookinete making a ring-like structure (indicated by arrows). Labelling with P28 was used to identify the surface of activated female gametes, zygotes and ookinetes and to mark these stages (red). DNA is labelled with Hoechst dye (blue) **(B)**. Ookinete developmental stages for *Δkinesin-20* and WTGFP parasites. Ookinetes were identified using P28 and defined as those cells differentiated successfully into elongated 'banana shaped' forms. Round cells are arrested zygotes or female gametocytes, while bulbous cells did not develop to banana-shaped ookinetes for *Δkinesin-20* parasites. DNA is stained with Hoechst dye (blue). Scale bar = 5 µm. **(C)** Ookinete conversion as a percentage of cells for *Δkinesin-20* and WTGFP parasites after 24 h. Mean ± SEM. n = 4 independent experiments. **(D)** Representative frames from time-lapse videos of motile WTGFP ookinetes and sessile ookinetes of *Δkinesin-20* in Matrigel. Black arrow indicates apical end of ookinete. Scale bar = 5 µm. **(E)** Ookinete

motility for WT-GFP and *Δkinesin-20* lines in Matrigel. More than 20 ookinetes were examined for each line**.** Mean ± SEM. n = 3 independent experiments. **(F)** Representative confocal images of expanded ookinetes of WTGFP and bulbous cells of *Δkinesin-20* lines stained for α- and β-tubulin (magenta) showing sub-pellicle MTs. Scale bar=1 µm. **(G)** The MT lengths were measured from the images of ookinetes stained to reveal α and β tubulins obtained by expansion microscopy. The bar diagram shows the length of subpellicular MTs in bulbous *Δkinesin-20* ookinetes compared to WTGFP ookinetes. Mean ± SEM. n = 3 independent experiments. Underlying data are provided in the Supporting information as S1 Data.

Fig 4. Ultrastructural analysis of WTGFP and *Δkinesin-20* ookinetes. (A) Electron micrographs of WTGFP **(a, d, f, h)** and *Δkinesin-20* **(b, c, e, g, i)** ookinetes. Bars represent 1 µm (a-c) and 100 nm (d-i). **(a)** Longitudinal section of a crescentic shaped WTGFP ookinete showing the apical complex (AC) with numerous micronemes (M) in the anterior cytoplasm and a more posteriorly located crystalline body (Cr) and nucleus (N). (**b)** Longitudinal section through an immature *Δkinesin-20* ookinete displaying a bulbous shape. Within the cytoplasm, the apical complex (AC) plus an irregular shaped nucleus (N) and a few irregularly arranged dense granules (DG) can be identified. (**c).** Longitudinal section through a more mature *Δkinesin-20* ookinete showing a bulbous shaped cell. Within the cytoplasm the apical complex (AC), nucleus (N) and crystalline body (Cr) can be identifying but note the micronemes (M) appear to be distributed throughout the cytoplasm. (**d, e)** Details of longitudinal sections through the apical complex of WTGFP **(d)** and *Δkinesin-20* **(e)** ookinetes showing similar substructures consisting of three conoidal rings (CR), an anterior polar ring 1 (P1) formed by the IMC and a second polar ring (P2) representing the initiation site for the sub-pellicular microtubules (Mt). The polar rings are separated by a collar consisting of an outer electron dense layer (cd) and an inner electron lucent layer (cl). Note the micronemes (M) with ducts (D) direct to the anterior plasmalemma. (**f, g)** Cross section through the periphery of the anterior complex of a WTGFP **(f)** and a *Δkinesin-20* **(g)** parasite showing similar sub-structure consisting of the outer plasmalemma (PM) and the underlying inner membrane complex (IMC) which appears fused to the outer electron dense (cd) region of the apical collar while the more electron lucent inner region is in close contact with sub-pellicular microtubules (Mt). **(h, i)** Cross section of the pellicle posterior to the apical complex consisting of the outer plasmalemma and the underlying IMC. Note that while the sub-pellicular microtubules (Mt) in the WTGFP parasite **(h)** are evenly spaced, those of the *Δkinesin-20* **(i)** show irregular spacing and some clumping. **(B)** A schematic diagram of ookinete showing the defects in microtubule organization posterior to apical complex. AC-apical complex, P1-polar ring 1**,** P2-polar ring 2, CR- conoidal rings, M-micronemes, Mt-microtubules, cd-dense layer, PM-plasmalemma

Fig 5. Kinesin-13 associates with kinetochore marker, NDC80, during various proliferative stages of parasite life cycle. Live cell imaging showing location of kinesin-13GFP (green) with respect to kinetochore marker NDC80Cherry (red) during asexual **(A, B)** and sexual **(C, D)** proliferative stages. Asexual proliferative stages include endomitosis during blood schizogony and sporogony. Sexual stages include endomitosis during male gametogenesis and meiosis during ookinete development. Kinesin-13GFP (green) shows a diffuse distribution in the cytoplasm, together with strong foci at different stages of development that co-localise with NDC80Cherry (red). DNA is stained with Hoechst dye (blue). Scale bar = 5 µm.

Fig 6. Kinesin-13 associates with axonemes in male gametocytes and gametes and its knockdown affects male gamete formation (A) Expansion microscopy showing co-localization of kinesin-13 (green) with α/β tubulin staining (purple) in gametocytes activated for 15 min. mpa = min post activation**.** Scale bar = 5 µm. **(B)** Indirect immunofluorescence assay showing the co-localisation of kinesin-13 (green) and tubulin (red) staining in male gamete. Scale bar = 5 µm. **(C)** qRTPCR analysis showing down-regulation of kinesin-13 gene in *kinesin-13PTD* parasites compared to WTGFP. Mean ± SEM, n=3 independent experiments. **(D)** Exflagellation centres per field at 15 min post-activation. n = 3 independent experiments (>20 fields per experiment). Error bar, ± SEM. **(E)** Percentage ookinete conversion from zygote. n= 3 independent experiments (> 80 cells). Error bar, ± SEM. **(F)** qRT-PCR analysis of transcripts for other kinesin genes in *kinesin-13PTD* compared to WTGFP parasites. n= 3 independent experiments. Error bar, ± SEM. **(G)** RNAseq analysis showing depletion of kinesin-13 transcript in *kinesin-13PTD* parasites**. (H)** Volcano plot showing differentially regulated genes in *kinesin-13PTD* gametocytes before activation (0 min). **(I)** Volcano plot showing differentially regulated genes in *kinesin-13PTD* gametocytes activated for 15 min. **(J)** Heat maps showing differential regulation of various genes involved in axoneme biogenesis, IMC/glideosome and chromosome dynamics**.** **p*≤0.05, ***p*≤0.01 and ****p*≤0.001. Underlying data are provided in the Supporting information as S2 Data.

Fig 7. Ultrastructural analysis of WTGFP and *kinesin-13PTD* gametocytes and ookinetes. (A) Representative confocal images of expanded gametocytes of WTGFP and *kinesin-13PTD* lines stained for α- and β-tubulin (magenta) showing labelling of spindle (arrow) and axonemal MTs (arrowhead) at 4-5 min and axonemal MTs (arrowhead) at 15 min post activation. Similarly, representative confocal images of expanded ookinetes of WTGFP and *kinesin-13PTD* lines stained for α- and β-tubulin (magenta) showing well-organised subpellicular MTs (white arrows) and apical tubulin ring (ATR, red arrows) in WTGFP ookinetes and disorganised MTs in *kinesin-13PTD* ookinetes. Scale bars = 1 µm. **(B)** Electron micrographs of *P. berghei* male gametogenesis of WTGFP **(a, b, e, f, g)** and *kinesin-13PTD* **(c, d, h, i)** at 6 min **(a – d)** and 15 min **(e – i)** post-activation. Bars represent 1 µm in **a, c, e, h** and 100 nm in other micrographs. **(a)** Early stage WTGFP showing the large central nucleus (N) displaying two nuclear poles (NP) with cytoplasm containing several axonemes (A). **(b)** Detail of the cytoplasm illustrating several normal 9+2 axonemes (A) and abnormal axonemes. **(c)** Early-stage *kinesin-13PTD* gametocytes showing the central nucleus (N) but the cytoplasm lacked visible axonemes. **(d)** Detail of the enclosed area in **c** showing randomly arranged free single and duplet MTs with some forming partial axonemes. **(e)** Late stage WTGFP showing a flagellum (F) of a developing microgamete emerging from the male gametocyte (exflagellation). N- nucleus; Ch- chromatin. **(f)** Detail of a longitudinal section through a free male gamete showing the nucleus (N) and flagellum (F). **(g)** Detail of a cross section through a male gamete showing the 9+2 flagellum and the nucleus (arrowhead). **(h)** Late-stage *kinesin-13PTD* gametocyte showing the central nucleus (N) with clumps of chromatin (Ch) but an absence of any 9+2 axonemes. **(i)** Detail of the enclosed area in **h** showing a microtubule (Mt) enclosed by the plasmalemma emerging from the male gametocyte.

Supplementary Materials

Supplementary figures

S1 Fig. Generation and genotypic analysis of kinesin-GFP parasites

A. Schematic representation of the endogenous *kinesin* locus, the GFP-tagging construct and the recombined *kinesin* locus following single homologous recombination. Arrows 1 (P1) and 3 (P3) indicate the position of PCR primers used to confirm successful integration of the construct. **B.** Diagnostic PCR of *kinesin* and WT parasites using primers: integration primer (P1) and ol492 (P2). The bands of expected size for amplified DNA fragments are indicated for each tagged line.

S2 Fig. Immunoprecipitation and mass-spectrometric analysis of kinesins

A. The number of peptides after immunoprecipitation using GFP-trap beads and their coverage to full length kinesins. Controls; WTANKA or non-kinesin-GFP parasites. **B.** Locations of peptides in full length kinesin proteins.

S3 Fig. Kinesin pattern of expression and diverse subcellular locations at various stages in the *Plasmodium berghei* life cycle

Live cell imaging showing subcellular locations of nine kinesin-GFP proteins (green) during various stages of the *P. berghei* life cycle*.* DNA is stained with Hoechst dye (blue)*.* Arrowhead indicates basal end and arrow indicates apical end of the ookinete. Mpa = min post activation. Oocyst-NS: non-sporulating oocyst, Oocyst-S: sporulating oocyst. Scale bar = 5 µm.

S4 Fig. Generation and genotypic analysis of Δ*kinesin* parasites

A. Schematic representation of the endogenous *kinesin* locus, the targeting knockout construct and the recombined *kinesin* locus following double homologous crossover recombination. Arrows 1 and 2 indicate PCR primers used to confirm successful integration in the *kinesin* locus following recombination and arrows 3 and 4 indicate PCR primers used to show deletion of the *kinesin* gene. **B.** Integration PCR of the *kinesin* locus in WTGFP (WT) and knockout (Mut) parasites using primers: integration primer and ol248. Integration of the targeting construct gives expected size band for each gene. **C.** qRT-PCR analysis of transcript in WT-GFP and Δ*kinesin* parasites confirming the deletion of respective genes.

S5 Fig. Phenotypic screen of nine kinesins in *Plasmodium* reveals their role during sexual and transmission stages within mosquito vector. A. Male gametogenesis in kinesin gene-deletion lines in comparison with WTGFP parasite, measured as the number of exflagellation centres per field; more than 20 fields were counted for each line**.** Mean ± SEM. n = 3 independent experiments. **B.** Percentage ookinete conversion comparing knockout and WTGFP parasites. Ookinetes were identified using 13.1 antibody for surface marker (P28, red) and defined as those cells that differentiated successfully into elongated 'banana shaped' ookinetes. Mean ± SEM. n = 5 independent experiments. **C.** Total number of GFP-positive oocysts per mosquito midgut at 7-, 14- and 21-days post infection for knockout and WTGFP parasites; at least 10 mosquito midguts were counted for each line. Mean ± SEM. n= 3 independent experiments. **D.** Representative mosquito midguts at 10x and 63x magnification showing oocysts of

kinesin knockout and WTGFP lines at 7-, 14- and 21-days post infection. Scale bar = 50 µm (10x), 20 µm (63x). **E.** Total number of sporozoites in oocysts of kinesin knockout and WTGFP parasites at 14- and 21-days post infection. Mean ± SEM. n = 3 independent experiments. **F.** Total number of sporozoites in salivary glands of kinesin knockout and WT-GFP parasites. Mean ± SEM. n = 3 independent experiments. **G.** Mosquito bite back experiments showing no transmission of *Δkinesin-8B* and *Δkinesin-8X* parasites, while other kinesin knockout and WTGFP parasites show successful transmission from mosquito to mice. Mean ± SEM. n = 3 independent experiments. **p*≤0.05, ***p*≤0.01 and ****p*≤0.001. Underlying data are provided in the Supporting information as S3 Data.

S6 Fig. The location of kinesin-5 and kinesin-8X in relation to that of kinetochore (NDC80) and axoneme marker (kinesin-8B).

A. Live cell images of gametocytes showing dual lines expressing either kinesin-5GFP or NDC80-mCherry/kinesin-8BmCherry or both in the same gametocyte. **B.** Live cell imaging showing the temporal dynamics of kinesin-5GFP (green) along with kinetochore marker NDC80Cherry (red) during male gametogenesis. DNA is stained with Hoechst dye (blue); mpa = min post activation; Scale bar=5 µm. **C.** The location of kinesin-5GFP (green) in relation to the axoneme marker, kinesin-8BCherry (red) during male gamete formation. **D.** The location of kinesin-8XGFP (green) in relation to the axoneme marker, kinesin-8BCherry (red) during male gamete formation. The nuclear location of kinesin-5 and kinesin-8X contrasts with the cytoplasmic location of kinesin-8B during chromosome replication and segregation, indicating that kinesin-5 and kinesin-8X are associated with the mitotic spindle. mpa = min post activation. DNA is stained with Hoechst dye (blue). Scale bar = 5 µm.

S7 Fig. ChIP-seq analysis of kinesin-8X and kinesin-5 during gametocyte stage.

Centromeric localization confirmed by ChIP-seq analysis of kinesin-8XGFP and kinesin-5GFP profiles for all 14 chromosomes in gametocyte stage. Signals are plotted on a normalized read per million (RPM) basis. Lines on top are division points between chromosomes and circles on the bottom indicate locations of centromeres. NDC80-GFP was used as a positive control and IgG was used as a negative control.

S8 Fig. qRT-PCR and RNA-seq analysis and sporozoite motility of *Δkinesin-20* parasite lines

A. Representative frames from time-lapse videos showing motile sporozoites of WTGFP and *Δkinesin-20* lines. Black arrow indicates the apical end of the sporozoites. Scale bar = 5 µm. **B.** Sporozoite motility for WTGFP and *Δkinesin-20* lines. More than 20 sporozoites were examined for each line**.** Mean ± SEM. n = 3 independent experiments. **C.** qRT-PCR analysis of transcripts for other kinesin genes in *Δkinesin-20* and WTGFP parasites. Mean ± SEM. n = 3 independent experiments. Ns = not significant. **D.** RNAseq analysis showing no transcript in *Δkinesin-20* parasites. **E.** Volcano plot showing differentially regulated genes in *Δkinesin-20* gametocytes activated for 2h. Underlying data are provided in the Supporting information as S4 Data.

S9 Fig. Generation and genotype analysis of *conditional knockdown kinesin-13* parasites

A. Schematic representation of auxin inducible degron (AID) strategy to generate *kinesin-13AID/HA* parasites. **B.** Integration PCR of the kinesin-13AID/HA construct in the

kinesin-13 locus. Oligonucleotides used for PCR genotyping are indicated and agarose gels for corresponding PCR products from genotyping reactions are shown. **C.** Kinesin-13AID/HA protein expression level as measured by western blotting upon addition of auxin to mature purified gametocytes; α-tubulin serves as a loading control. **D.** Schematic representation of the promoter swap strategy (*kinesin-13PTD*, placing *kinesin-13* under the control of the *clag* promoter) by double homologous recombination. Arrows 1 and 2 indicate the primer positions used to confirm 5' integration and arrows 3 and 4 indicate the primers used for 3' integration. **E.** Integration PCR of the promotor swap construct into the *kinesin-13* locus. Primer 1 (5'-IntPTD50) with primer 2 (5'-IntPTD) were used to determine successful integration of the selectable marker. Primer 3 (3'-intClag) and primer 4 (3'-IntPTD50) were used to determine the successful integration of the *clag* promoter. Primer 1 (5'-IntPTD50) and primer 4 (3'-IntPTD50) were used to show complete knock-in of the construct and the absence of a band at 2.3 kb (endogenous) expected if no integration occurred. **F.** Oocysts at days 7, 14, and 21 post infection. n = 3 independent experiments with a minimum of 8 mosquito guts. Error bar, ± SEM. **G.** Bite back experiments reveal no transmission of *kinesin-13PTD* and successful transmission of WTGFP parasites from mosquito to mouse. Mean ± SEM. n = 3 independent experiments. Underlying data are provided in the Supporting information as S5 Data.

Supplementary Tables

S1 Table. List of genes differentially expressed between Δ*kinesin-20* and WTGFP activated gametocytes for 2h (S1A table); and between *kinesin-13PTD* and WTGFP gametocytes (S1B table and S1C table)

S2 Table. Oligonucleotides used in this study.

Supplementary Movies

S1 Movie: Gliding motility of WT-GFP ookinetes
S2 Movie: Gliding motility of *Δkinesin-20* ookinetes
S3 Movie: Gliding motility of WT-GFP salivary gland sporozoite
S4 Movie: Gliding motility *Δkinesin-20* salivary gland sporozoite

S1 data: Excel spreadsheet containing the underlying numerical data for Fig 3 C, G and E.
S2 data: Excel spreadsheet containing the underlying numerical data for Fig 6 C, D, E and F.
S3 data: Excel spreadsheet containing the underlying numerical data for Fig S5 A, B, C, E, F and G.
S4 data: Excel spreadsheet containing the underlying numerical data for Fig S8 B and C.
S5 data: Excel spreadsheet containing the underlying numerical data for Fig S9 F and G.

S1 Raw Images. Original gel and blot images.

Fig 1

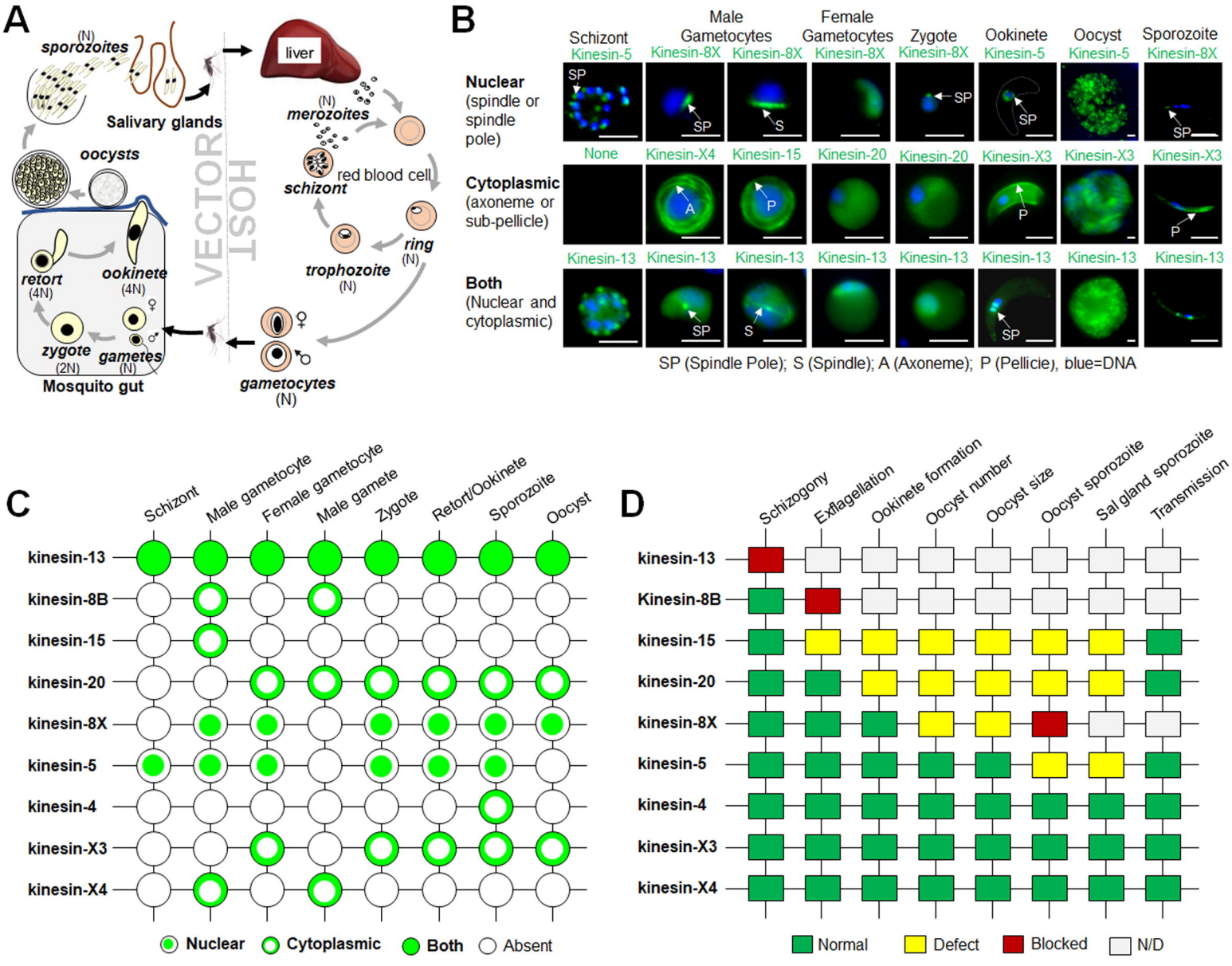
A
(N)
sporozoites
Salivary glands
liver
(N)
merozoites
red blood cell
schizont
ring
(N)
trophozoite
(N)
oocysts
VECTOR
HOST
retort
(4N)
ookinete
(4N)
zygote
(2N)
gametes
(N)
Mosquito gut
gametocytes
(N)
B
Schizont
Male Gametocytes
Female Gametocytes
Zygote
Ookinete
Oocyst
Sporozoite
Nuclear (spindle or spindle pole)
Kinesin-5
Kinesin-8X
Kinesin-8X
Kinesin-8X
Kinesin-8X
Kinesin-5
Kinesin-5
Kinesin-8X
SP
SP
S
SP
SP
SP
Cytoplasmic (axoneme or sub-pellicle)
None
Kinesin-X4
Kinesin-15
Kinesin-20
Kinesin-20
Kinesin-X3
Kinesin-X3
Kinesin-X3
A
P
P
P
Both (Nuclear and cytoplasmic)
Kinesin-13
Kinesin-13
Kinesin-13
Kinesin-13
Kinesin-13
Kinesin-13
Kinesin-13
Kinesin-13
SP
S
SP
SP (Spindle Pole); S (Spindle); A (Axoneme); P (Pellicle), blue=DNA
C
Schizont
Male gametocyte
Female gametocyte
Male gamete
Zygote
Retort/Ookinete
Sporozoite
Oocyst
kinesin-13
kinesin-8B
kinesin-15
kinesin-20
kinesin-8X
kinesin-5
kinesin-4
kinesin-X3
kinesin-X4
Nuclear
Cytoplasmic
Both
Absent
D
Schizogony
Exflagellation
Ookinete formation
Oocyst number
Oocyst size
Oocyst sporozoite
Sal gland sporozoite
Transmission
kinesin-13
Kinesin-8B
kinesin-15
kinesin-20
kinesin-8X
kinesin-5
kinesin-4
kinesin-X3
kinesin-X4
Normal
Defect
Blocked
N/D

Fig 2

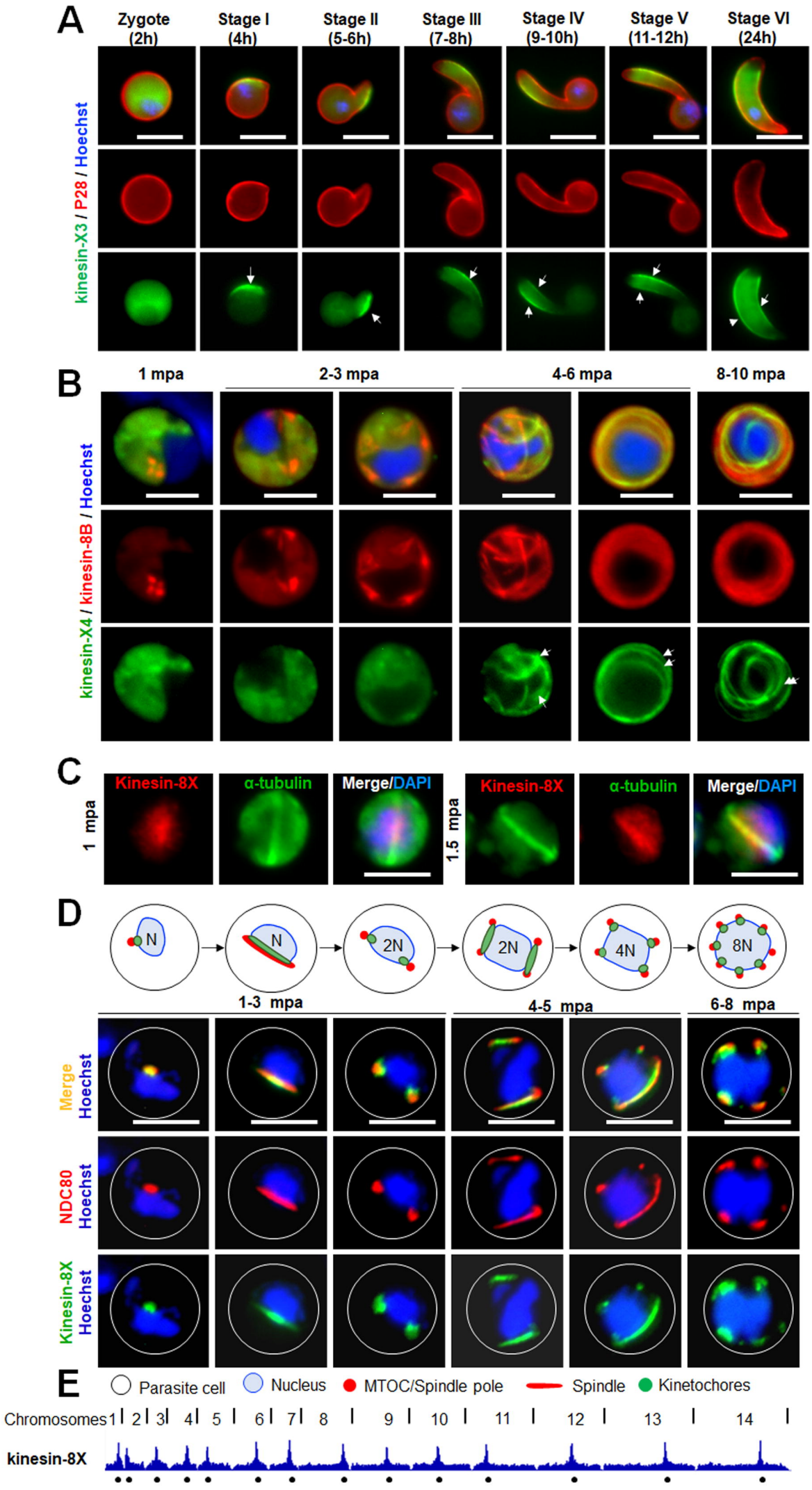
A
Zygote (2h)
Stage I (4h)
Stage II (5-6h)
Stage III (7-8h)
Stage IV (9-10h)
Stage V (11-12h)
Stage VI (24h)
kinesin-X3 / P28 / Hoechst
B
1 mpa
2-3 mpa
4-6 mpa
8-10 mpa
kinesin-X4 / kinesin-8B / Hoechst
C
1 mpa
Kinesin-8X
α-tubulin
Merge/DAPI
1.5 mpa
Kinesin-8X
α-tubulin
Merge/DAPI
D
N
N
2N
2N
4N
8N
1-3 mpa
4-5 mpa
6-8 mpa
Merge Hoechst
NDC80 Hoechst
Kinesin-8X Hoechst
E
Parasite cell
Nucleus
MTOC/Spindle pole
Spindle
Kinetochores
Chromosomes 1 2 3 4 5 6 7 8 9 10 11 12 13 14
kinesin-8X

Fig 3

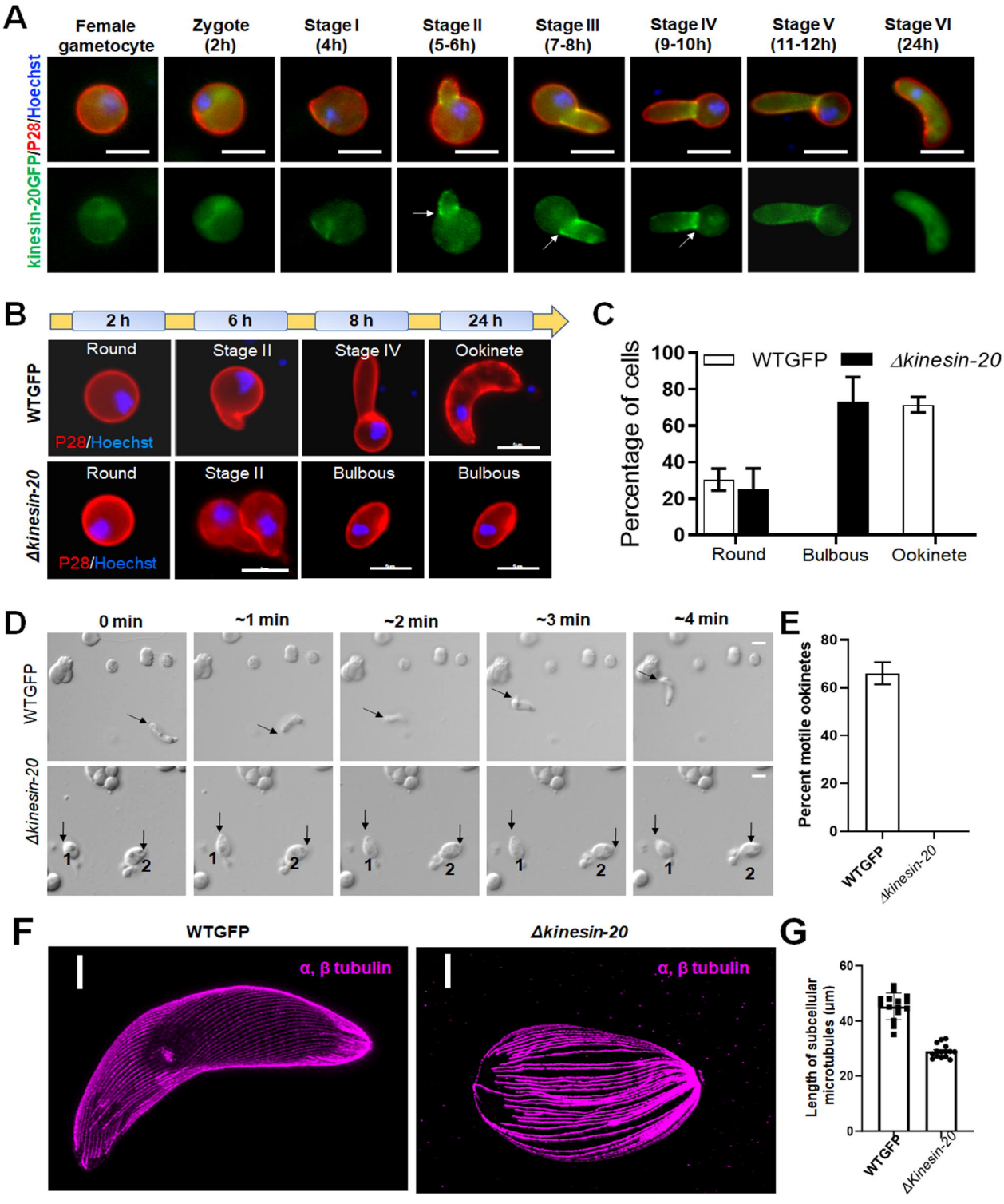
A
Female gametocyte
Zygote (2h)
Stage I (4h)
Stage II (5-6h)
Stage III (7-8h)
Stage IV (9-10h)
Stage V (11-12h)
Stage VI (24h)
kinesin-20GFP/P28/Hoechst
B
2 h
6 h
8 h
24 h
WTGFP
Round
Stage II
Stage IV
Ookinete
P28/Hoechst
Δkinesin-20
Round
Stage II
Bulbous
Bulbous
P28/Hoechst
C
WTGFP
Δkinesin-20
Percentage of cells
100
80
60
40
20
0
Round
Bulbous
Ookinete
D
0 min
~1 min
~2 min
~3 min
~4 min
WTGFP
Δkinesin-20
1
2
E
Percent motile ookinetes
80
60
40
20
0
WTGFP
Δkinesin-20
F
WTGFP
Δkinesin-20
α, β tubulin
α, β tubulin
G
Length of subcellular microtubules (μm)
60
40
20
0
WTGFP
ΔKinesin-20

Fig 4

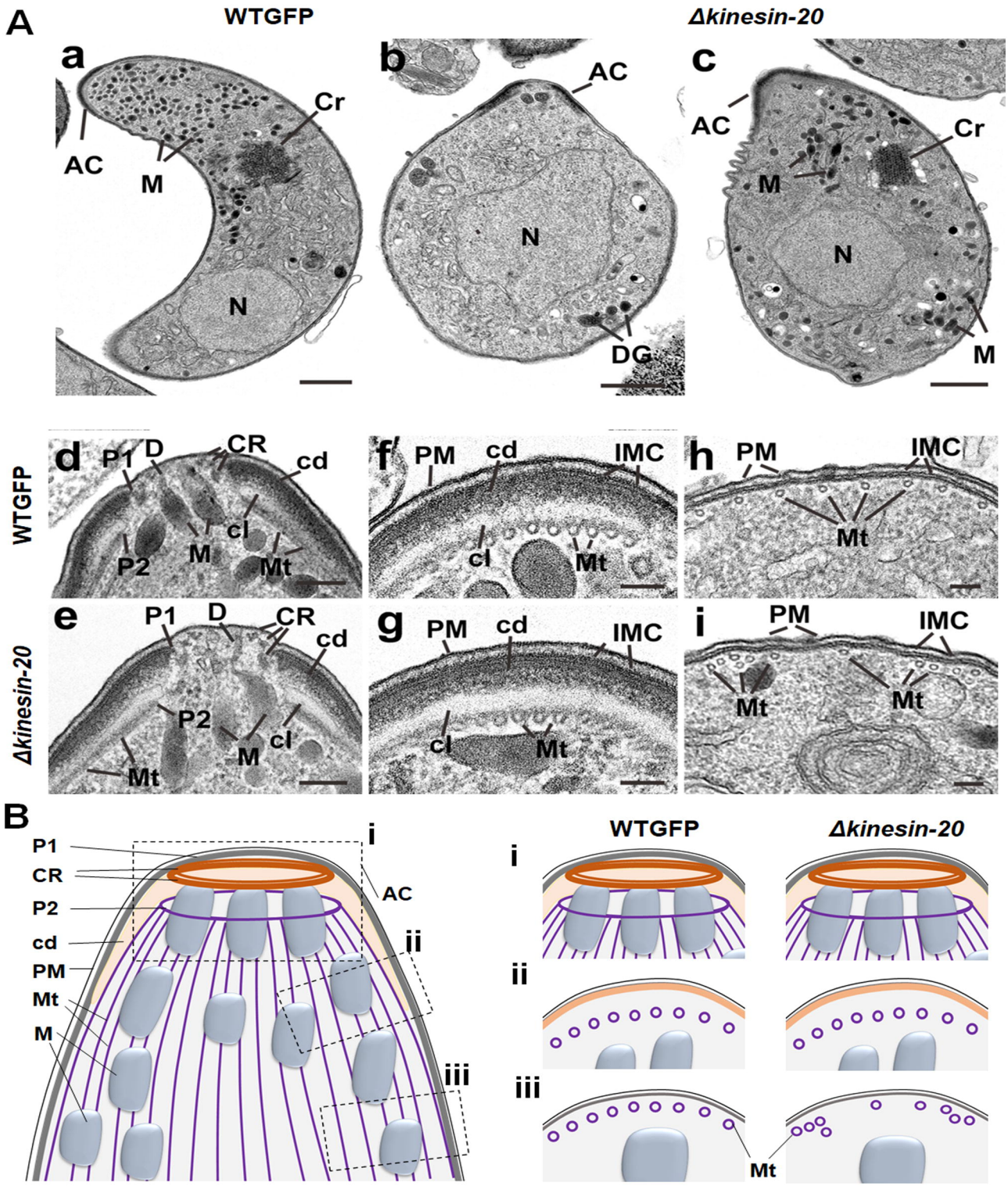
A
WTGFP
Δkinesin-20
a
AC
M
Cr
N
b
AC
N
DG
c
AC
Cr
M
N
M
WTGFP
d
P1
D
CR
cd
P2
M
cl
Mt
f
PM
cd
IMC
cl
Mt
h
PM
IMC
Mt
Δkinesin-20
e
P1
D
CR
cd
P2
M
cl
Mt
g
PM
cd
IMC
cl
Mt
i
PM
IMC
Mt
Mt
B
P1
CR
P2
cd
PM
Mt
M
i
AC
ii
iii
WTGFP
Δkinesin-20
i
ii
iii
Mt

Fig 5

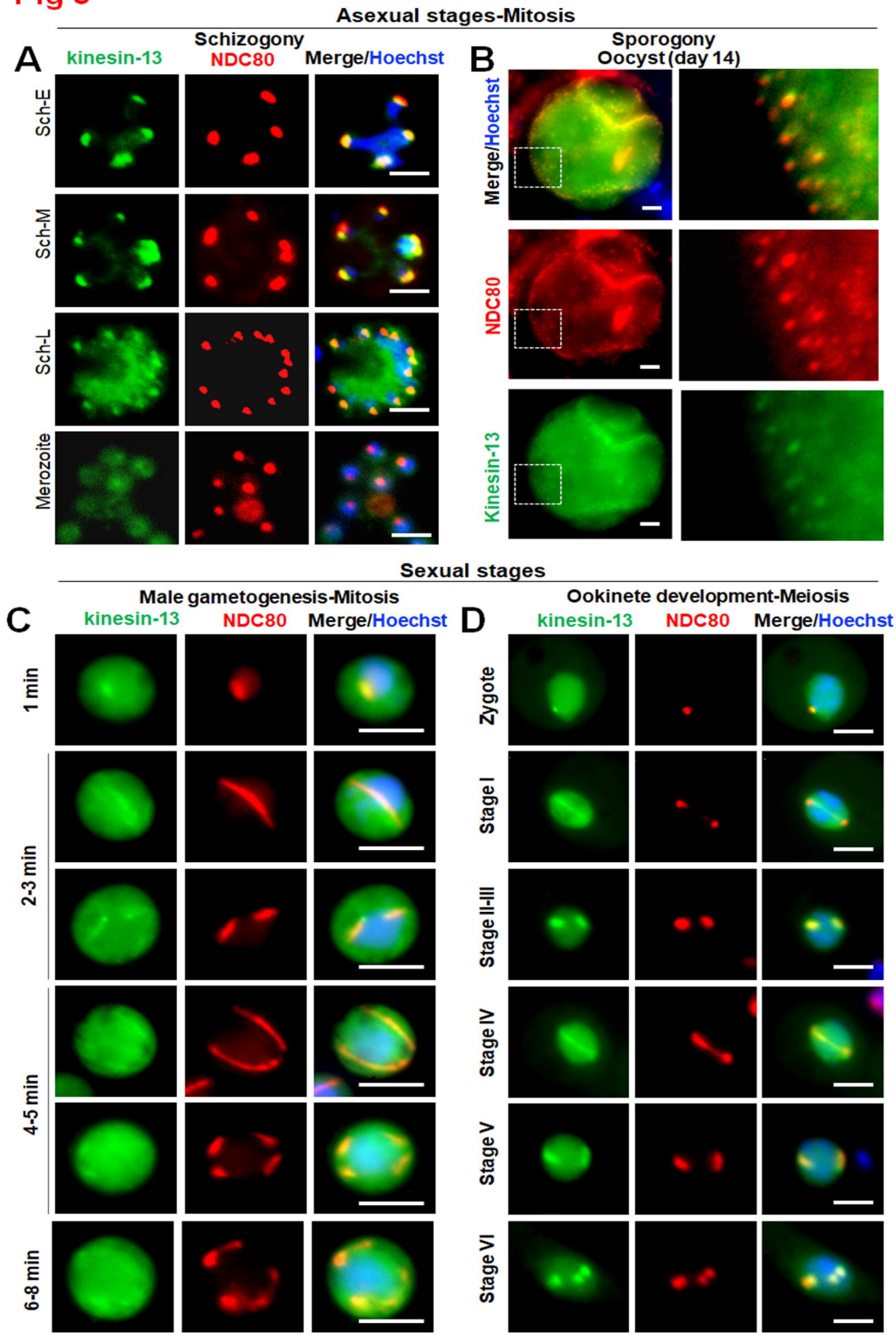
Asexual stages-Mitosis
A
Schizogony
kinesin-13
NDC80
Merge/Hoechst
Sch-E
Sch-M
Sch-L
Merozoite
B
Sporogony
Oocyst (day 14)
Merge/Hoechst
NDC80
Kinesin-13
Sexual stages
C
Male gametogenesis-Mitosis
kinesin-13
NDC80
Merge/Hoechst
1 min
2-3 min
4-5 min
6-8 min
D
Ookinete development-Meiosis
kinesin-13
NDC80
Merge/Hoechst
Zygote
Stage I
Stage II-III
Stage IV
Stage V
Stage VI

Fig 6

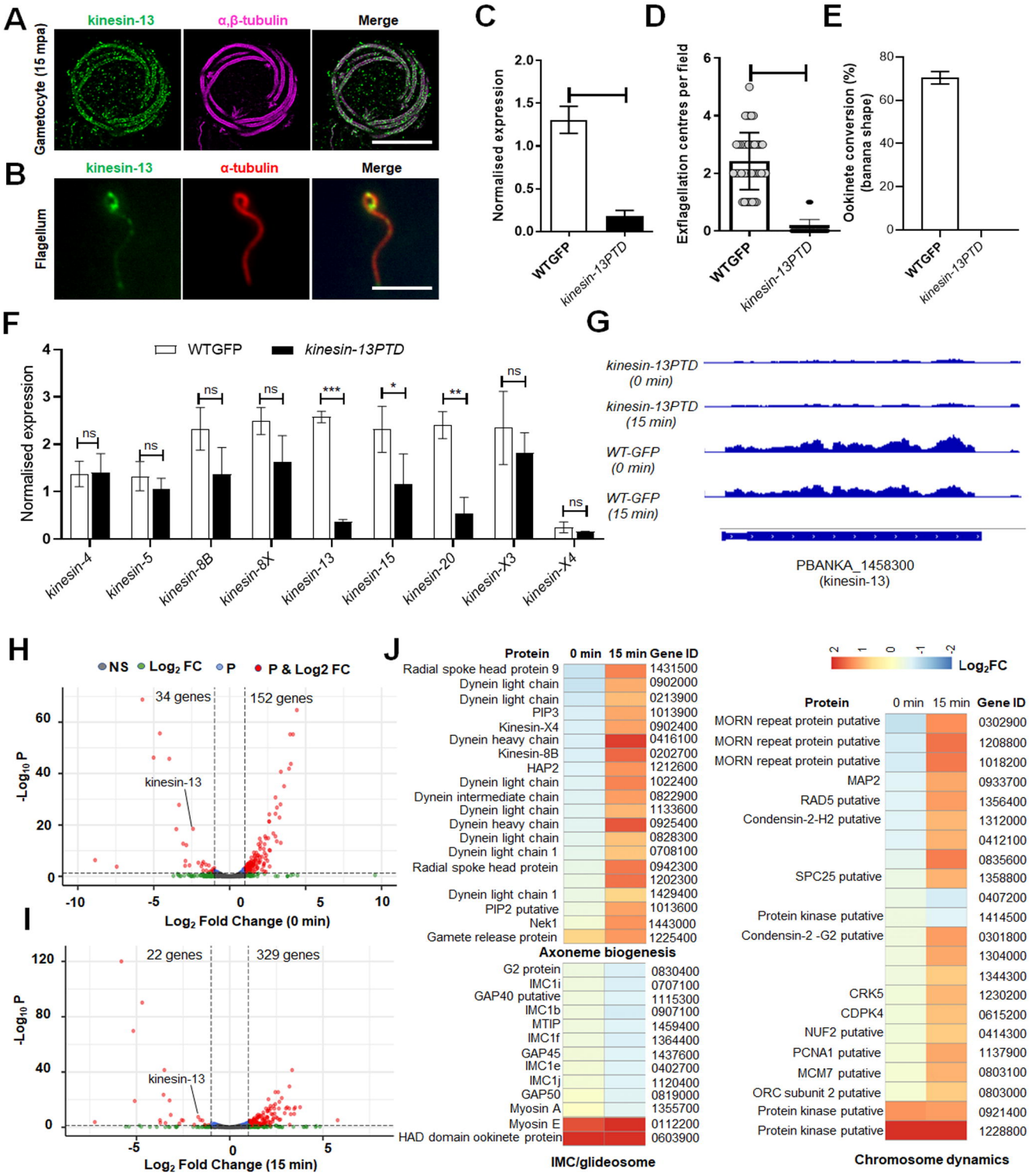
A
kinesin-13
α,β-tubulin
Merge
Gametocyte (15 mpa)
B
kinesin-13
α-tubulin
Merge
Flagellum
C
Normalised expression
WTGFP
kinesin-13PTD
D
Exflagellation centres per field
WTGFP
kinesin-13PTD
E
Ookinete conversion (%) (banana shape)
WTGFP
kinesin-13PTD
F
WTGFP
kinesin-13PTD
Normalised expression
ns
***
*
**
kinesin-4
kinesin-5
kinesin-8B
kinesin-8X
kinesin-13
kinesin-15
kinesin-20
kinesin-X3
kinesin-X4
G
kinesin-13PTD (0 min)
kinesin-13PTD (15 min)
WT-GFP (0 min)
WT-GFP (15 min)
PBANKA_1458300 (kinesin-13)
H
NS
Log2 FC
P
P & Log2 FC
34 genes
152 genes
kinesin-13
-Log10 P
Log2 Fold Change (0 min)
I
22 genes
329 genes
kinesin-13
-Log10 P
Log2 Fold Change (15 min)
J
Protein
0 min
15 min
Gene ID
Radial spoke head protein 9 1431500
Dynein light chain 0902000
Dynein light chain 0213900
PIP3 1013900
Kinesin-X4 0902400
Dynein heavy chain 0416100
Kinesin-8B 0202700
HAP2 1212600
Dynein light chain 1022400
Dynein intermediate chain 0822900
Dynein light chain 1133600
Dynein heavy chain 0925400
Dynein light chain 0828300
Dynein light chain 1 0708100
Radial spoke head protein 0942300
1202300
Dynein light chain 1 1429400
PIP2 putative 1013600
Nek1 1443000
Gamete release protein 1225400
Axoneme biogenesis
G2 protein 0830400
IMC1i 0707100
GAP40 putative 1115300
IMC1b 0907100
MTIP 1459400
IMC1f 1364400
GAP45 1437600
IMC1e 0402700
IMC1j 1120400
GAP50 0819000
Myosin A 1355700
Myosin E 0112200
HAD domain ookinete protein 0603900
IMC/glideosome
Log2FC
Protein
0 min
15 min
Gene ID
MORN repeat protein putative 0302900
MORN repeat protein putative 1208800
MORN repeat protein putative 1018200
MAP2 0933700
RAD5 putative 1356400
Condensin-2-H2 putative 1312000
0412100
0835600
SPC25 putative 1358800
0407200
Protein kinase putative 1414500
Condensin-2 -G2 putative 0301800
1304000
1344300
CRK5 1230200
CDPK4 0615200
NUF2 putative 0414300
PCNA1 putative 1137900
MCM7 putative 0803100
ORC subunit 2 putative 0803000
Protein kinase putative 0921400
Protein kinase putative 1228800
Chromosome dynamics

Fig 7

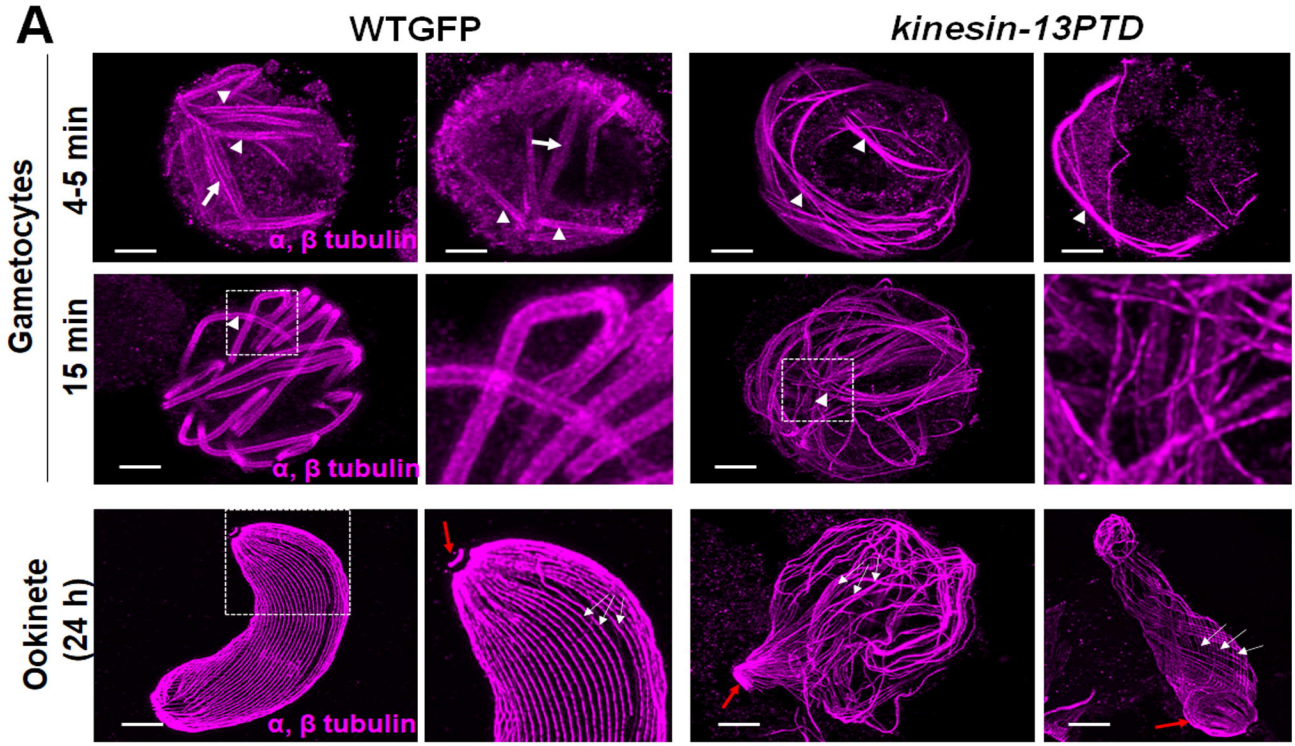
A
WTGFP
kinesin-13PTD
Gametocytes
4-5 min
15 min
Ookinete (24 h)
α, β tubulin

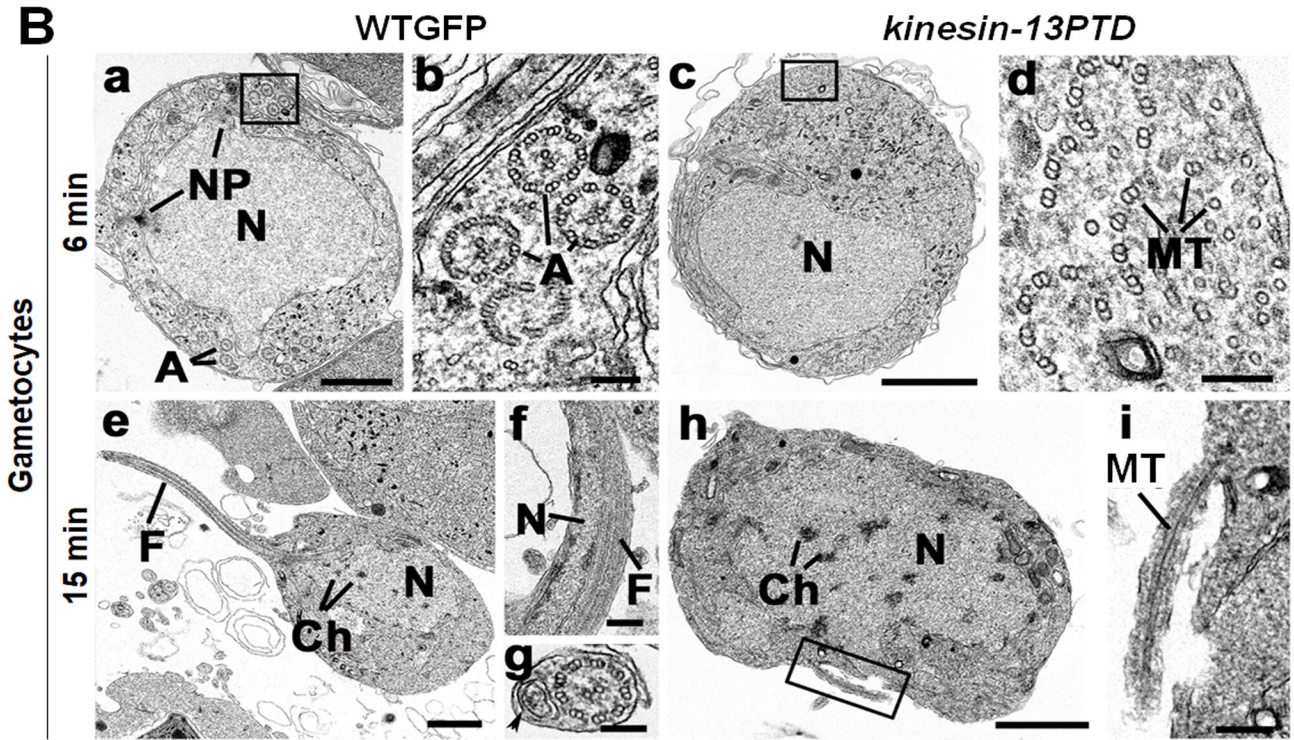
B
WTGFP
kinesin-13PTD
Gametocytes
6 min
15 min
a
b
c
d
e
f
g
h
i
NP
N
A
MT
F
Ch